A model for fluids in metamorphosed ultramafic rocks : observations at surface and subsurface conditions (high pH spring waters)

Autor(en): **Pfeifer, Hans-Rudolf**

Objekttyp: **Article**

Zeitschrift: **Schweizerische mineralogische und petrographische Mitteilungen = Bulletin suisse de minéralogie et pétrographie**

Band (Jahr): **57 (1977)**

Heft 3

PDF erstellt am: **29.06.2024**

Persistenter Link: https://doi.org/10.5169/seals-44441

Schweiz. mineral. petrogr. Mitt. 57, 361–396, 1977

A Model for Fluids in Metamorphosed Ultramafic Rocks

Observations at Surface and Subsurface Conditions (High pH Spring Waters)

By *Hans-Rudolf Pfeifer* (Zürich)*)

Abstract

Subsurface waters issuing from ultramafic rocks all over the world show unusually high pH values. Two compositional groups can be distinguished: (1) high Mg and Si, carbonate as the dominant anion, pH 9–11, found both in peridotite and serpentinite areas (Mg-HCO_3-type); (2) high Ca, low Mg and Si, hydroxyl ion as the major anion and normally no carbonate, pH 11–12, usually only found in peridotite areas (Ca-OH-type). A saturation test shows that both waters reflect their parent rock composition: Both are highly supersaturated with respect to most low temperature Mg- and Ca-Mg-silicates (chrysotile, talc, sepiolite, diopside, tremolite, etc.). Their relatively narrow composition range can nevertheless be explained with buffering by silica and carbonate minerals for Mg-HCO_3-waters, and by forsterite, in part by enstatite, a Ca-silicate and a hypothetical high soluble serpentine phase for Ca-OH-waters. Observed water compositions can be reproduced by a quantitative computer simulation of a rock dissolution process by meteoric water (rain water like) at 20° C, 1 bar. These computations suggest that: (1) the high pH-values observed are due to the fact that saturation values for most Mg- and Ca-Mg-silicates lie in the high pH-region and are reached through hydrolysis-type dissolution reactions which consume H^+, (2) silica minerals (quartz, etc.) do only form if the fluid contains CO_2, (3) Mg-HCO_3-waters can form by two different mechanisms: through interaction with a serpentinite rock close to the surface or through mixing of a Ca-OH-water from a peridotite with atmospheric CO_2 and subsequent calcite-precipitation, (4) Ca-OH-waters can form by dissolution of a Ca-bearing peridotite, either directly from CO_2-poor rainwater or through a Mg-HCO_3- stage by loosing CO_2 through carbonate mineral precipitation. High Ca reflects the inability to reach clinopyroxene- or calcite-saturation (disequilibrium and lack of CO_2 respectively). Ca-OH-waters represent a highly metastable state and are therefore less commonly found in nature.

A. Introduction

Various field and phase equilibrium studies in metamorphosed ultramafic rocks have shown that already a few percent CO_2 in a H_2O-dominated fluid are

*) Institut für Kristallographie und Petrographie, ETH-Zentrum, CH-8092 Zürich, Switzerland.

sufficient to dissolve anhydrous and hydrous silicates and convert them into carbonate minerals and more silica-rich phases (GREENWOOD, 1967; JOHANNES, 1969; TROMMSDORFF and EVANS, 1977). Furthermore, the occurrence of hydrogen gas at some spring localities in ultramafic rocks (BARNES and O'NEIL, 1969) and petrological reasoning (common occurrence of magnetite-rich spinell in ultramafics) suggest that reducing conditions are predominant in these fluids. Despite these many studies, little is known about aqueous species concentrations like H^+, OH^-, Mg, Ca (free ions and complexes), SiO_2, etc., which are undoubtedly present in these fluids in the whole range of metamorphic conditions (HELGESON, 1967, 1970; EUGSTER, 1977).

There are four major methods to provide more data on these fluid solution parameters in metamorphic ultramafic rocks: (1) experiments involving minerals and fluid solutions (see references in MOODY, 1976; POTY et al., 1972; HEMLEY et al., 1977a, b), (2) studies of natural active fluid-rock systems (geothermal wells, mineral springs), (3) fluid inclusion studies (ROEDDER, 1965, 1972) and (4), petrological studies of fossil fluid-rock systems (metamorphic rocks) combined with theoretical interpretation based mainly on thermodynamic theory of electrolyte solutions (HELGESON and KIRKHAM, 1974a, b, 1976).

A combination of (2) and (4), based on the presently available observations and thermodynamic data, allows a good prediction for "ultramafic" fluids under metamorphic conditions. It also allows a useful comparison of the predicted parameters with a still active and explorable part of this fluid-rock system. Data on an active low temperature fluid-ultramafic rock system (spring waters) are used to find the relevant parameters and reaction mechanisms for the chosen electrolyte-type fluid solution model. On the basis of these observations made at low temperatures and pressures, it is planed to use the same model for the metamorphic region, by taking into account all theoretically predictable changes in the fluid with increasing P and T. Such changes involve the increasing association of free ions to ion pairs or complexes and the (normally) decreasing log K-values for silicate hydrolysis equilibria (HELGESON and KIRKHAM, 1976; HELGESON, 1969).

This paper deals only with the low temperature observations and is in part an extension of the earlier work done by BARNES and O'NEIL (1969), and BARNES et al. (1972). First, all available geological and chemical data on surface and subsurface waters issuing from ultramafic rocks are compiled and compared. Second, an equilibrium model for the aqueous fluid is used for a saturation test of these waters with respect to minerals of the ultramafic system and to determine possible control factors and reaction mechanisms. Third, these results are then used in a fluid-rock dissolution model, in which the fluid is treated with the same equilibrium model as before, to explain how these waters reached their characteristic compositions. However, the overall irreversible dis-

solution process is only treated with equilibrium thermodynamics, that is, rates and transport processes are not explicitely considered.

B. Geological features of high pH-waters from ultramafics

Table 1 is a list of water samples to be considered and summarizes available geological data. Samples 1–5 represent new data, the rest is compiled from the literature. Two main rock groups are distinguished: (1) largely serpentinized ultramafics ("serpentinites") and (2) only slightly serpentinized ultramafics ("peridotites, dunites", including pyroxenites and hornblendites).

C. Chemical and physical features

Table 2 summarizes the chemical and physical properties of the 23 waters under consideration. Among samples 1 to 20, obviously two groups can be distinguished: (1) sample 2–15 with pH 9–11, carbonate present, high SiO_2- and Mg- and low Ca-contents (Mg-HCO_3-waters, BARNES and O'NEIL, 1969), (2) sample 1 and 16–20 with pH 11–12, no carbonate present, low SiO_2- and Mg- and high Ca-contents (Ca-OH-waters). A comparison with the related rock types (table 1) shows that group (1) occurs in both peridotites and serpentinites, but group (2) usually only in peridotites. Thus, the presence of CO_2 in the solution seems to be an important factor. Stable isotope data for samples 6, 7 and 12–20 and the geological situation of 1–5 and 8–11 suggest a meteoric origin of those waters. Samples 21–23 are at least partly non-meteoric (BARNES et al., 1972) and form a separate group which has only its pH-values in common with the other samples but otherwise is less influenced by ultramafic rocks (Na-Cl-HCO_3-waters).

D. Saturation state of the waters (equilibrium model for the fluid)

1. THE MODEL

The fact that a fluid solution is saturated with respect to certain minerals can reveal possible relations between rocks and fluids. In order to determine the degree of saturation (saturation test), the activities of the uncomplexed fluid species must be known, which in turn can be calculated with an equilibrium model from analytical concentrations. Several computer programs exist for such a fluid species distribution calculation (BARNES and CLARKE, 1969; SOLSAT: LEEPER, 1969, HELGESON et al., 1970; SOLMNEQ: KHARAKA and

Table 1. General geological characteristics of high pH-waters issuing from ultramafic rocks

Sample 1–5 are published for the first time, 6–23 are from the literature. Mineral abbreviations in third column: Chr chrysotile, Liz lizardite, Ant antigorite, Arag aragonite, Di diopside, Ol olivine, Br brucite, Px pyroxene, Carb carbonate minerals in general, Mag magnesite, Hydromag hydromagnesite, Dol dolomite. Remarks: [1]) Swiss coordinates 814.650/183.730, 1390 m above sea level, amount of water issuing per minute: 6 liter. [2]) 783.025/131.925, 1480 m, a few milliliters/min. [3]) 790.150/ 129.400, 1600 m, 5 liter/min. [4]) 790.000/129.200, 1600 m, 2–5 liter/min. [5]) 788.350/132.925, 2080 m, 2 liter/min. [6]) According to terminology of BARNES and O'NEIL (1969) and BARNES et al. (1972).

No.	Name	Location/ tectonic unit	Rock type in area feeding the spring	Source of water	Deposits at spring locality	pH	CO_3^{2-}	Water[6]) type	References for chemistry/geology
1	Val Plavna	Val Plavna, Engadine valley, Switzerland/Engadine window	Serpentinite (Chr, Liz), Di, Arag + Mag + Dol ± Qz on joints and in veins	Spring (fissure)	Calcite, dolomite, aragonite	10.8	Yes	Ca-OH	This paper/CADISCH, EUGSTER and WENK (1968); DE QUERVAIN (1976), FEHLMANN (1919)
2	Senevedo	Val Malenco, N. Italy/Malenco-Ultramafics[2])	Gneiss, serpentinite (Ant, Ol, Di, ± Br)	Spring in swamp	–	10.6	Yes	Mg-HCO_3	This paper/BUCHER and PFEIFER (1973); GRAMACCIOLI (1962)
3	Franscia 1	Val Malenco, N. Italy/Malenco-Ultramafics[3])	Serpentinite (Ant, Ol, Di, ± Br)	Spring in Alluvium	–	9.1	Yes	Mg-HCO_3	This paper/BUCHER and PFEIFER (1973); GRAMACCIOLI (1962)
4	Franscia 2	Val Malenco, N. Italy/Malenco-Ultramafics[4])	Serpentinite (Ant, Ol, Di, ± Br)	Spring in Alluvium	–	9.0	Yes	Mg-HCO_3	This paper/BUCHER and PFEIFER (1973); GRAMACCIOLI (1962)
5	Scerscen	Val Malenco, N. Italy/Malenco-Ultramafics[5])	Serpentinite (Ant, Ol, Di, ± Br), Chr-asbestos + andradite in veins	Creek in mine	Nesquehonite, hunite, calcite ± artinite, hydromag., siderite, talc	9.0	Yes	Mg-HCO_3	This paper/BUCHER and PFEIFER (1973); GRAMACCIOLI (1962)
6	Table Mountain A	Monterey Co., Calif. USA/Coast Ranges	Serpentinite	Spring	?	8.97	Yes	Mg-HCO_3	BARNES and O'NEIL (1969)
7	New Idria B	Fresno Co., Calif. USA/Coast Ranges	Serpent. (Chr ± Br), hydromag., calcite veins	Creek at mine locality	?	8.88	Yes	Mg-HCO_3	BARNES and O'NEIL (1969)
8	Lake Roland	Maryland, USA/ Appalachians	Serpentinite (Chr, Liz)	?	?	8.3	Yes	Mg-HCO_3	NESBITT (1974)
9	Soldiers Delight	USA/Appalachians	Serpentinite (Chr, Liz)	?	?	7.9	Yes	Mg-HCO_3	NESBITT (1974)

10	Dyer Quarry	USA/Appalachians	Serpent. (Chr, Liz)	?	?	8.67	Yes	Mg-HCO_3	Nesbitt (1974)
11	Cedar Hill	Piedmont, Penn. USA	Serpent. (Ant, $\pm$Br, $\pm$Chr)	?	?	8.78	Yes	Mg-HCO_3	Nesbitt (1974)
12	Burro Mountain A	Monterey Co., Calif. USA/Coast Ranges	Peridotites, dunites (Ol, Px, Chr, $\pm$Br)	Spring in Alluvium	Nesquehonite	8.15	Yes	Mg-HCO_3	Barnes and O'Neil (1969, 1971)
13	Cazadero B	Sonoma Co., Calif. USA/Coast Ranges	Peridotites, dunites (Ol, Px, Chr, $\pm$Br)	Creek	Nesquehonite	8.87	Yes	Mg-HCO_3	Barnes and O'Neil (1969, 1971)
14	John Day Ray Ranch	Grant Co., Oreg. USA/Canyon Mt. Complex	Peridotites, dunites (Ol, Px, Chr, $\pm$Br)	Spring	?	7.84	Yes	Mg-HCO_3	Barnes and O'Neil (1969)
15	Red Mountain Adobe Creek	Stanislaus Co., Calif. USA/Coast Ranges	Peridotites, dunites (Ol, Px, Chr, $\pm$Br, hydromag.)	Creek	Nesquehonite	8.88	Yes	Mg-HCO_3	Barnes and O'Neil (1969, 1971)
16	Burro Mountain B	Monterey Co., Calif. USA/Coast Ranges	Peridotites, dunites (Ol, Px, Chr, $\pm$Br)	Springs and seeps	Calcite-travertine	11.54	No	Ca-OH	Barnes and O'Neil (1969, 1971)
17	Cazadero A	Sonoma Co., Calif. USA/Coast Ranges	Peridotites, dunites (Ol, Px, Chr, $\pm$Br)	Seep	Calcite, aragonite-scum a. travertine	11.77	No	Ca-OH	Barnes and O'Neil (1969, 1971)
18	John Day Warm Spring	Grant Co., Oreg. USA	Peridotites, dunites (Ol, Px, Chr, $\pm$Br)	Spring	Calcite-scum	11.25	No	Ca-OH	Barnes and O'Neil (1969, 1971)
19	Red Mountain Adobe Canyon	Stanislaus Co., Calif. USA/Coast Ranges	Peridotites, dunites (Ol, Px, Chr, Br), hydromag., carb. in veins	Springs and seeps	?	11.78	No	Ca-OH	Barnes and O'Neil (1969, 1971)
20	Red Mountain Blackbird Valley	Sta. Clara Co., Calif. USA/Coast Ranges	Peridotites, dunites (Ol, Px, Chr, Br), hydromag., carb. in veins	Spring	Calcite-scum a.-travertines	12.01	No	Ca-OH	Barnes and O'Neil (1969, 1971)
21	Complexon Spring	Lake Co., Calif. USA/Coast Ranges	Serpent. (Chr, Liz), rodingites	Spring	Brucite-gel B-rich Si-gel	12.07	Yes	Na-Cl-HCO_3-	Barnes et al. (1972)
22	TC-2	Trinity Co., Calif. USA/Coast Ranges	Serpent. (Ant.) dacites	Spring along fault contact	Magadiite, kenyaite, rohdesite, mountainite, talc, tremolite, B-rich Si-gel	10.8	Yes	Na-Cl-HCO_3-	Barnes et al. (1972)
23	Aqua de Ney	Siskiyou Co., Calif. USA/Coast Ranges	Serpent. (Ant.) dacites	Spring along fault contact	B-rich Si-gel	10.9	Yes	Na-Cl-HCO_3-	Barnes et al. (1972)

Table 2. Chemical analyses of high pH-waters as totals in mg/liter and some parameters used in or resulting from fluid species distribution calculations

References see table 1. NA: not analysed. Analysis 1 was done by T. S. PRESSER, chemist U.S. Geol. Survey, Menlo Park, California; analyses 2–5: EAWAG, Dübendorf, Switzerland (done with standard analytical methods similar to those in chapt. 27 of *Schweizerisches Lebensmittelbuch*, 1972). Remarks: [1]) Field measurements. [2]) The sample which the presented analysis is based on did not contain carbonate. However an earlier partial analysis had carbonate (pH 10.1, 104 mg/l CO_3^{2-}, O. HÖGL, Univ. Bern, pers. communication 1974). [3]) Determined on the basis of the calculated species distribution. [4]) Temperature used to calculate species distribution.

No.	Name	pH	Temp. [°C]	Ca^{2+}	Mg^{2+}	Na^+	K^+	Cl^-	SO_4^{2-}	H_2S	CO_3^{2-}
				[milligrams/liter]							
1	Val Plavna	10.8	6	63	0.14	29	1.5	49	44	NA	102[2])
2	Senevedo	10.6[1])	8.7	8.4	0.24	119	6.7	81	9	NA	122
3	Franscia 1	9.1[1])	4	8.16	116.7	1.1	0.57	3.4	21	NA	551
4	Franscia 2	9.0	5	12.0	77.82	7.3	1.6	12	18	NA	372
5	Scerscen	9.0[1])	1.8	4.0	51.07	2.1	0.75	2.0	17	NA	232
6	Table Mt. A	8.97[1])	30	7.9	260	10	0.3	34	13	NA	1,437
7	New Idria B	8.88[1])	16	9.1	223	14	1.9	18	26	NA	1,150
8	Lake Roland	8.3	15	9.5	51	4.0	2.2	12	2.6	NA	271
9	Soldiers Delight	7.9	15	3.04	31.8	1.16	0.3	23	19.8	NA	138
10	Dyer Quarry	8.76	15	5.4	25	1.7	0.4	3.4	9.5	NA	96
11	Cedar Hill	8.78	15	2.6	67	3.8	0.6	10	19	NA	276
12	Burro Mt. A	8.15[1])	26.7	14	72	5.5	0.7	12	5.4	NA	431
13	Cazadero B	8.87[1])	23.5	2.9	40	3.6	0.2	5.8	0.4	NA	215
14	John Day Ray Ranch	7.84[1])	14.4	10	58	2.6	0.5	0	0.6	NA	324
15	Red Mountain Adobe Creek	8.88[1])	22	3.3	103	7.6	0.4	5.0	22.0	NA	509
16	Burro Mt. B	11.54[1])	20	40	0.3	19	1.1	6.3	0.4	NA	0
17	Cazadero B	11.77[1])	18	53	0.3	50	1.2	55	0	NA	0
18	John Day Warm Spring	11.25[1])	31	35	0.1	33	2.3	19	0	0.4	0
19	Red Mountain Adobe Canyon	11.78[1])	15.6	48	0.4	40	1.1	32	1.4	NA	0
20	Red Mountain Blackbird Valley	12.01[1])	10.6	51	0.06	22	0.54	26	0.5	0.1	0
21	Complexon Spring	12.07[1])	10	0.7	0.8	12,000	350	18,200	60	0	985
22	TC-2	10.8	10	1.2	0.2	7,550	210	7,500	132	74	4,270
23	Aqua de Ney	10.9	10	0.6	0.3	11,300	220	7,500	123	430	6,025

Fe^{2+}	Mn^{2+}	Al	SiO_2	OH^-	B	NH_3	O_2aq.	Calcul. log pCO_2[3]) [p in bar]	Calcul. ionic strength[3]) [mole/kg H_2O]	Temp. calc.[4]) [°C]
			[milligrams/liter]							
0	NA	0	43	36	NA	NA	<0.5	−6.58[2])	6.2×10^{-3}	5
<0.02	<0.01	0	34	2	NA	0.8	7.8	−6.04	6.9×10^{-3}	10
<0.02	0.01	0	5	0.05[3])	NA	0.73	11.1	−3.58	1.2×10^{-2}	5
<0.02	<0.01	0	4	0.04[3])	NA	4.65	NA	−2.52	9.4×10^{-3}	5
<0.02	0.01	0	0.6	0.02[3])	NA	0.12	NA	−3.62	5.7×10^{-3}	0
NA	0	0	31	0.28	0.4	0.17	NA	−2.96	2.3×10^{-2}	25
0	0.01	0	17	0.08	2.3	0.1	NA	−3.02	2.2×10^{-2}	15
NA	NA	0	31	0.02[3])	NA	1.86	NA	−2.96	6.9×10^{-3}	15
NA	NA	0	21	0.008[3])	NA	0.32	NA	−2.85	4.3×10^{-3}	15
NA	NA	0	14	0.05[3])	NA	1.59	NA	−3.78	3.5×10^{-3}	15
NA	NA	0	10	0.08[3])	NA	2.41	NA	−3.47	7.7×10^{-3}	15
0.01	0.02	0	22	0.031	0.1	0.23	NA	−2.53	9.9×10^{-3}	25
0	0.04	0	5.4	0.123	0.02	0	NA	−3.57	4.9×10^{-3}	25
0	0.02	0	32	0.006	0	0.01	NA	−2.43	7.8×10^{-3}	15
0.02	0.0	0	5.7	0.12	0.06	0	NA	−3.30	1.1×10^{-2}	20
0	0.02	0.2	0.4	42.8	0.02	0.19	NA	0	3.8×10^{-3}	20
0	0.05	0	0.3	62.3	0.01	0.1	NA	0	6.1×10^{-3}	20
0	0.01	0.7	5.9	50.5	0.1	0.2	NA	0	4.0×10^{-3}	25
0	0.02	0.4	5.2	51.9	0.1	0.2	NA	0	5.3×10^{-3}	15
<0.5	0	0.1	3.2	57.0	0.06	0.21	NA	0	6.0×10^{-3}	10
0	NA	NA	24	92	20	210	NA	−8.66	5.2×10^{-1}	10
0.13	NA	NA	765	4.8	130	121	NA	−5.34	3.5×10^{-1}	10
0.3	NA	NA	4,000	6	303	169	NA	−5.54	5.0×10^{-1}	10

BARNES, 1973; WATEQ: TRUESDELL and JONES, 1974, PLUMMER, TRUESDELL and JONES, 1976; EQUIL: FRITZ, 1975, DROUBI, FRITZ and TARDY, 1976; EQ3: WALTERS and WOLERY, 1975). Here, SOLSAT was used, in order to be consistent with the program for the numerical treatment of dissolution processes, which will be used later (PATH, PATHCALC).

A summary of basic assumptions and equations of SOLSAT is given in appendix 1 and is thought as a base for comparison with other above cited programs. In contrast to e.g. WATEQ, SOLSAT is based on a consistent set of thermodynamic data for aqueous species (HELGESON, 1969). However, the activity coefficient calculations are based on NaCl as the supporting electrolyte,

Table 3A. Three examples of species distributions calculated with program SOLSAT, based on the chemical analyses in table 2 (mg/l)

	9 Soldiers Delight	3 Franscia 1	19 Red Mountain Adobe Canyon
Al^{3+}	0.29	0.57	1.3×10^{-22}
K^+	0.29	0.57	1.09
Na^+	1.16	1.09	39.98
Ca^{2+}	2.90	6.72	46.43
Mg^{2+}	30.77	82.74	0.23
Mn^{2+}	–	0.01	0.02
SiO_2 aq.	20.65	4.04	0.04
HS^-	$<10^{-10}$	$<10^{-10}$	$<10^{-10}$
SO_4^{2-}	17.85	17.98	1.23
CO_3^{2-}	0.46	20.81	–
Cl^-	5.32	3.40	45.12
OH^-	0.006	0.03	47.01
H^+	1.4×10^{-5}	8.8×10^{-6}	1.79×10^{-9}
KSO_4^-	9×10^{-4}	0.001	2×10^{-4}
$NaCl^\circ$	5×10^{-5}	4×10^{-5}	0.02
$NaCO_3^-$	3×10^{-4}	0.006	–
$NaSO_4^-$	0.007	0.005	0.02
$CaCO_3^\circ$	0.004	2.69	–
$CaHCO_3^+$	0.14	0.63	–
$CaSO_4^\circ$	0.22	0.37	0.22
$Ca(OH)^+$	2×10^{-5}	1.6×10^{-4}	2.16
$MgCO_3^\circ$	1.21	112.0	–
$MgHCO_3^+$	0.74	3.01	–
$MgSO_4^\circ$	2.23	3.43	0.001
$Mg(OH)^+$	0.005	0.05	0.28
$MnSO_4^\circ$	–	3×10^{-4}	6×10^{-5}
$H_3SiO_4^-$	0.54	1.52	8.2
HSO_4^-	1×10^{-5}	7×10^{-7}	1×10^{-10}
S^{2-}	$<10^{-10}$	$<10^{-10}$	$<10^{-10}$
H_2S°	$<10^{-10}$	$<10^{-10}$	$<10^{-10}$
HCO_3^-	134.34	453	–
$H_2CO_3^*$	3.68	0.78	–
HCl	$<10^{-10}$	$<10^{-10}$	$<10^{-10}$
$Al(OH)^{2+}$	–	–	6.5×10^{-16}
$Al(OH)_4^-$	–	–	1.41
$AlSO_4^+$	–	–	10^{-20}
pCO_2	$10^{-2.8}$	$10^{-3.6}$	0
pO_2	10^{-65}	10^{-68}	10^{-68}

Table 3B. Complex-formation of major ions in percent

Complexing is quite considerable, especially for the carbonate bearing waters (all except 1, 16–20).

No.	Name	Ca	Mg	Na	K	Al	Fe	Mn
1	Val Plavna	4.23	6.63	0.25	0.15	–	–	–
2	Senevedo	42.06	61.30	0.78	0.4	–	–	–
3	Franscia 1	17.64	29.05	0.23	0.06	–	–	1.11
4	Franscia 2	12.28	19.98	0.17	0.06	–	–	–
5	Scerscen	59.14	75.21	0.85	0.06	–	–	1.21
6	Table Mountain A	46.00	51.9	1.27	0.04	–	–	–
7	New Idria B	28.04	37.3	0.5	0.07	–	–	–
8	Lake Roland	6.07	6.20	0.05	0.01	–	–	–
9	Soldiers Delight	4.53	3.19	0.13	0.08	–	–	–
10	Dyer Quarry	4.68	5.66	0.09	0.04	–	–	–
11	Cedar Hill	11.07	14.48	0.2	0.07	–	–	–
12	Burro Mountain A	11.37	9.91	0.11	0.02	–	34.38	0.36
13	Cazadero B	14.06	17.71	0.19	0.002	–	–	0.04
14	John Day Ray Ranch	5.06	3.49	0.02	0.002	–	–	0.04
15	Red Mountain Adobe Creek	21.38	27.41	0.4	0.08	–	69.4	1.35
16	Burro Mountain B	3.03	30.64	0.008	0.002	100	–	0.04
17	Cazadero A	4.78	52.80	0.007	0	–	–	0
18	John Day Warm Spring	2.44	36.03	0.01	0	100	–	0
19	Red Mountain Adobe Canyon	3.29	41.95	0.02	0.006	100	–	0.11
20	Red Mountain Blackbird Valley	3.37	43.04	0.03	0.002	100	–	–
21	Complexon Spring	33.03	64.91	4.41	0.04	–	–	–
22	TC-2	75.37	88.78	8.68	0.11	–	98.09	–
23	Acqua de Ney	75.38	89.22	9.73	0.08	–	98.37	–

redox reactions are calculated from sulphide-sulphate reactions (which are influenced by organic activity at low temperature) instead of O_2 aq.-measurements and the calculations are only done for a discrete P,T-net (5°–25° C intervalls).

Equations and data for the considered equilibria are given in appendix 2 and 3. The following minerals could not be considered because appropriate thermodynamic data are lacking: lizardite, most zeolites, most Ca-silicate hydrates (Taylor, 1968; Harnik and Harnik, 1976). Instead of the latter, portlandite, wollastonite and monticellite have been used, although they might only metastably exist at these low pressures and temperatures, but serve as substituts for any type of Ca-silicate.

2. RESULTS OF THE SATURATION TEST

General remarks: Three typical calculated species distributions and the calculated complexing of all waters are given in table 3. The results of the saturation test are given in table 4 (details in appendix 4). Because of the many uncertainties in this approach (reaction of water when reaching the surface, chemical analysis, equilibrium assumption for the fluid, thermodynamic data, especially activity coefficients), a deviation of up to 1000 cal/mole for $\Delta(\Delta G_r)$ (ap-

Table 4. Summary of observed saturation states of waters issuing from ultramafic rocks with respect to Fe-Al-free phases

Compare with appendix 4. ○: close to saturation, ●: supersaturation, empty: undersaturation.

Mineral	Serpentinites (chrysotile/ lizardite and antigorite)											Slightly serpentinized peridotites and dunites									mixed sources		
	1	2	3	4	5	6	7	8	9	10	11	12	13	14	15	16	17	18	19	20	21	22	23
Antigorite	●	●	●	●		●	●	●		●	●	●	●		●	●	●	●	●	●	●	●	●
Brucite																●	●	○	●	○	●		
Halite																							
Sylvite																							
Calcite		●	○	●	●	●	●	○		○	○	○	○	○							○	○	○
Magnesite			○	●	●	●	●	○	○	○	●	●	●	○	○						○		○
Dolomite		●	●	●	●	●	●	●	○	●	●	●	●	●	●						●	●	●
Hydromagnesite						●	○																
Anhydrite																							
Gypsum																							
Quartz	○	○	○	○	○	○	○	●	●	○	○	○	○	●	○							●	●
Sepiolite	●	●	●	●		●	●	●		●	●	●	●	○	○			●	●	○	●	●	●
Chrysotile	●	●	●	●		●	●	●		●	●	●	●		●	●	●	●	●	●	●	●	●
Chrysotile-asbestos						○					●					○	○	○	●	○			○
Talc	●	●	●	●	○	●	●	●	●	●	●	●	●	●	●	●	●	●	●	●	●	●	●
Artinite						○															○		
Tremolite	●	●	●	●		●	●	●		●	●	●	●			●	●	●	●	●	●	●	●
Enstatite	○					○	○											○	○		○	○	○
Diopside	●	●				●	○									●	●	●	●	●	●	●	●
Wollastonite	○																	○	○	○			
Forsterite																○	○	○	●	○	●		●
Huntite			●	●	●		●	○			●	●	●										
Amorphous silica								○	○					○								○	○
Nesquehonite																							
Aragonite		●	○	○	●	●	●	○		○	○	○	○	○							○	○	○
Periclase																							
Chalcedony	○	○	○	○		○	○	○	○	○	○	○	○		○							●	●
Mg-Anthophyllite	●	●	●		●	●					●	○	●					●	●	●	●	●	●
Merwinite																							
Monticellite																○	●	●	●	●			
Akermanite																							
Hexahedrite																							
Epsomite																							
Kenyaite																						○	●
Magadiite																						●	●
Rhodochrosite			○	●									○		○								
Portlandite																							

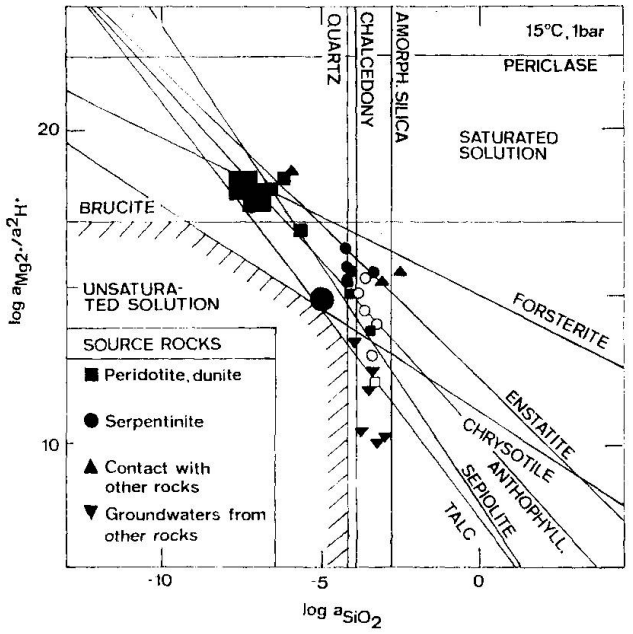

Fig. 1. Calculated free silica- and Mg-activities of 23 "ultramafic" water samples and their relative saturation state with respect to Mg-silicates, shown on a logarithmic activity diagram. Note: The saturation lines are drawn for a mean temperature (15° C) and do only in some cases correspond exactly to the measured temperatures of the waters (open symbols). The size of the symbols corresponds to the estimated analytical uncertainties. There are obviously two major groups of compositions: one close to the saturation lines of silica minerals (Mg-HCO_3-waters) and one close to forsterite saturation (Ca-OH-waters). Mean groundwater compositions from other rocks plot, with a few exceptions, at lower $a_{Mg^{2+}}/a^2_{H^+}$-rations.

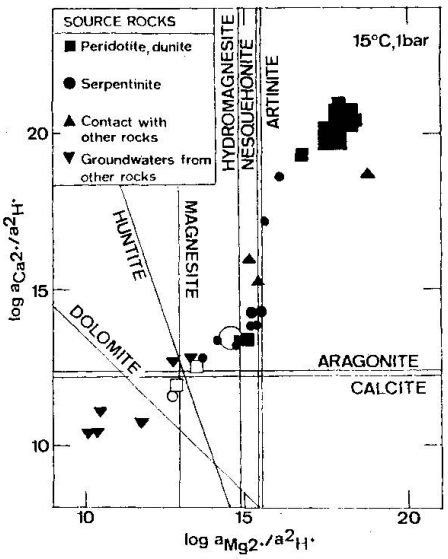

Fig. 2. Calculated free Ca^{2+}- and Mg^{2+}-activities and some carbonate mineral saturation lines. As the shown points correspond to different temperatures and f_{CO_2}-values, the shown lines, which are for $f_{CO_2} = 10^{-2.5}$ bar, 15° C, only correspond exactly to the *open* symbols. For other conditions, the lines would show parallel displacement.

pendix 1 and 4) was allowed for saturation. Unfortunately Fe- and Al-concentrations were often below detection limit for most waters (0.02 and 0.1 mg/liter respectively). For this reason important minerals like magnetite, zeolites and clay minerals could only in a few cases be checked for saturation (appendix 4B and C). Fig. 1 is a *graphical* representation of some of the calculated free ion concentrations and the corresponding degree of saturation with respect to Mg-silicates. Fig. 2 shows similar relations for carbonate minerals. An inspection of these tables and graphs clearly shows that the previously distinguished water types also show distinct saturation conditions, however, in part metastable ones.

Mg-HCO_3-waters (sample 2–15) seem to have their composition determined by being close to saturation with respect to silica minerals, like quartz, chalcedony and amorphous silica (possibly determining SiO_2) and carbonate min-

erals such as calcite/aragonite and magnesite (determining Ca and Mg). Only a few show saturation with hydromagnesite, hunite and artinite. Their carbonate content varies considerably (log pCO_2 in table 2). About half of the samples seem to be close to equilibrium with atmospheric CO_2 (log $pCO_2 \approx -3.5$), others seem to be determined by organic activity (log $pCO_2 > -3.5$). In sample 12 saturation with goethite seems to determine the Fe-content. However, most samples are strongly supersaturated with respect to common hydrous Mg- and Ca-Mg-silicates of ultramafic rocks, such as serpentines, talc, sepiolite, anthophyllite, tremolite. Also quite typical is the supersaturation with respect to dolomite.

Ca-OH-waters (sample 1, 16–20): Most of them seem to be close to saturation with forsterite and some also with enstatite and wollastonite, which determine Mg, SiO_2 and Ca in the fluid. Al-bearing samples show saturation with gibbsite. However, most samples are supersaturated with respect to brucite. Also typical is their quite strong supersaturation with diopside, tremolite and monticellite.

Na-Cl-HCO_3-waters (sample 21–23) usually stem from contacts with other rock types and exhibit less clear saturation conditions. As outlined by Barnes et al. (1972), they might be of rather complex origin (mixture of meteoric water influenced by ultramafics and non-meteoric water).

Groundwaters from other rock types (cf. figs. 1 and 2) show in most cases distinctly different compositions and saturation states than waters from ultramafic areas.

The redox state of these waters is commonly difficult to determine because only a few O_2 aq. measurements or simultaneous SO_4^{2-} and HS^- determinations are available for the considered waters. Most Mg-HCO_3-waters are probably saturated with atmospheric O_2 which had access after they reached the surface. This effect also keeps soluble Fe^{2+} often below the detection limit (0.02 mg/l). However, the few cases in which the redox state could approximately be calculated from SO_4^{2-}/HS^- data (sample 18, 20, 22, 23: pO_2 between 10^{-76} and 10^{-80} bar) and the fact that H_2 gas was reported from Burro Mountain (sample 16), indicate an originally reducing character of the fluid, especially for the Ca-OH-type. For water in equilibrium with olivine, orthopyroxene and spinel a theoretical redox state can be calculated e.g. from the equilibrium:

$$3\,Fe_2SiO_4 \text{ (in Olivine)} + H_2O = Fe_3O_4 \text{ (in spinell)} + 3\,FeSiO_3 \text{ (in opx)} + H_2 \text{ (gas)}$$

$$2\,H_2O = 2\,H_2 + O_2$$

assuming the presence of magnetite (R. Garrels, pers. communication). If data from Helgeson, Delany and Nesbitt (1977) are used, the calculated pH_2 is about 10^{-2} atm and pO_2 about 10^{-80} atm (no correction for solid solution made). High SO_4^{2-} contents in the Mg-HCO_3-waters could be the product of pyrite-oxidation.

3. CONCLUSIONS FROM THE SATURATION TEST

Both the Mg-HCO_3 and the Ca-OH-water type are potentially able to precipitate those minerals which usually form part of the ultramafic source rock (chrysotile, talc). The first type could, in addition, form ophicarbonate (TROMMSDORFF and EVANS, 1977; FOLK and MCBRIDGE, 1976) and silica-carbonate rocks (magnesite-opal/chalcedony, e.g. BODENLOS, 1949; BARNES et al., 1973), both often found low temperature alteration products of ultramafic rocks. However, with a few exceptions (samples 21–23), only carbonates have been found as coatings and other spring deposits (table 1). Apparently all of these water-types, though saturated or supersaturated with respect to these minerals, do not precipitate quartz, chrysotile-serpentine, brucite, talc, sepiolite, tremolite and Ca-silicates, probably mainly for kinetic reasons.

One might also ask whether the in part quite high supersaturation could not be attributed to insufficiency of the model. The lack of reliable thermodynamic data for many low temperature silicate-hydrates, fine-grained precursors and gels, with which the solutions might be in equilibrium, and the neglect of certain components (e.g. Al), could lead to serious misinterpretations (apparent disequilibrium states). On the other hand the presence of not considered fluid complexes can be excluded. For some minerals constant supersaturation values can be observed, e.g. for portlandite, nesquehonite, and especially for chrysotile. A steady disequilibrium state or a displaced equilibrium state can be used as explanation. Such a displacement can be caused by surface energy effects (fine-grained precursors) or by impurity effects (a solid solution phase precipitates instead of a pure phase). For both effects reliable data are largely missing. Appendix 4D shows an attempt to consider solid-solution effects (Fe-Mg in silicates, Ca-Mg in carbonates). Although the used data are rather hypothetical, it seems that solid solution effects cannot compensate the observed supersaturation with pure phases.

For chrysotile, another hypothesis is proposed. The occurrence of fine-grained chrysotile-asbestos on joint surfaces in most ultramafic rocks suggests a formation at moderately low temperatures and pressures. Although, it could not be proved yet for surface conditions, it is suggested as a working hypothesis, that the observed formal "supersaturation" could possibly represent the equilibrium point with a fine-grained impure serpentine phase such as chrysotile-asbestos. As will be shown later, such a displaced saturation boundary for serpentine could nicely explain the evolution of high pH-waters through dissolution of adjacent ultramafic rocks. Therefore, the hypothetical phase "chrysotile-asbestos", with a log K-hydrolysis value of 38.88, corresponding to 10 kcal supersaturation for normal chrysotile, has been included in the saturation test (table 4 and appendix 4) and in the following dissolution computations.

E. A fluid rock-interaction model for the formation of low temperature "ultramafic" fluids

1. INTRODUCTION (SIMULATION OF DISSOLUTION AND MIXING PROCESSES)

As most of the investigated Mg-HCO_3- and Ca-OH-waters are of local meteoric origin, it seems reasonable to look at a water-rock interaction process, in which surface water (e.g. rain-water with low or high CO_2, depending on the usually thin soil layer) enters an ultramafic rock body, starts dissolving the rock in a pervasive joint and fault system and comes up to the surface, wherever the local situation is suitable, and equilibrates with the atmosphere.

Thus, modeling of such processes involves a dissolution and a mixing part (with the atmosphere). As the following calculations show, it is possible to get a Ca-OH-water from rock/rain water-interaction through a "Mg-HCO_3"-stage close to surface where air still influences the dissolution process. On the other hand, Mg-HCO_3-waters can be explained as Ca-OH-waters equilibrated with atmospheric CO_2 and O_2. Both processes seem to work in nature.

2. DISSOLUTION CALCULATIONS

The calculations were again done with a computer program (PATH 3, a modified version of PATHCALC or PATH, Helgeson, 1968, Helgeson et al., 1970, Helgeson et al., 1971; analogue to program DISSOL, Fritz, 1975; Droubi, Fritz and Tardy, 1976) of which the fluid solution model corresponds exactly to the one used previously in program SOLSAT (appendix 1). Since program PATH is best described in terms of the equations on which it is based (see references given above), only a short qualitative description is given in appendix 5. All of the following calculations were performed at 20° C and 1 bar.

In order to separate the influence of the many factors which determine such a fluid rock interaction process (composition of reacting rock, CO_2-content of the fluid, kinetics which lead to supersaturation, open or closed system, i.e. iso- or non isochemical process), two main groups of model calculations were performed: (1) simple model, assuming equilibrium among fluid species and partial (local) equilibrium among fluid species and new forming (precipitating) minerals during the dissolution process, i.e. a stable equilibrium model, in which reaction paths follow stable saturation curves or surfaces in activity diagrams (see below), and which does not consider supersaturation, (2) improved model, in which for some minerals reaction paths follow stable or metastable equilibrium (saturation-) curves, for others disequilibrium is allowed. Thus, this model *considers* supersaturation.

For each model various rock types and initial fluid compositions were used (combinations see table 5). With one exception the fluid compositions used to start with correspond to a rain water dominated fluid as the major element concentrations are concerned. The mean rain water composition of GARRELS and MACKENZIE (1971) has been modified for this purpose in the following way: CO_3^{2-} and SO_4^{2-} (as totals) have been chosen within the limits observed in natural

Table 5 A. Model rock compositions for which dissolution calculations have been performed

No.	Composition		
Monomineralic rocks		*Model-peridotites*	
R 1	100% forsterite	R 5	90% forsterite, 8% enstatite, 2% diopside
R 2	100% chrysotile	R 6	70% forsterite, 10% enstatite, 20% diopside
R 3	100% enstatite	R 7	80% forsterite, 10% enstatite, 10% diopside
R 4	100% talc		
Model-serpentinites			
R 8	90% chrysotile, 10% diopside		
R 9	85% chrysotile, 5% diopside, 10% brucite		
R 11	70% chrysotile, 30% diopside		
Sligthly serpentinized peridotites (model)			
R 10	70% forsterite, 15% chrysotile, 5% diopside, 10% brucite		

Table 5 B. Fluid compositions which were used as initial solutions in dissolution calculations (with program PATH 3), mg/l

	F1[1])	F2[2])	F3[3])	F4[3])	F5[4])	F6[5])	F7[6])
pH	5.7	5.7	5.7	5.7	5.7	5.7	6.5
Ca^{2+}	1.3	1.3	1.3	1.3	1.3	1.3	40
Mg^{2+}	0.4	0.4	0.4	0.4	0.4	0.4	2.5
Na^{+}	3.5	3.5	3.5	3.5	70	690	70
K^{+}	2.0	2.0	2.0	2.0	20	390	20
Cl^{-}	20	20	20	20	20	20	20
SO_4^{2-}	15	15	15	15	15	15	15
HS^{-}	3.3×10^{-6}	3.3×10^{-6}	3.3×10^{-6}	3.3×10^{-6}	3.3×10^{-6}	3.3×10^{-6}	3.3×10^{-6}
CO_3^{2-}	–	3	10	30	246	1,436	246
SiO_2 aq.	6×10^{-6}	6×10^{-6}	6×10^{-6}	6×10^{-6}	6×10^{-6}	6×10^{-6}	0.6

[1]) No CO_3. [2]) Very low CO_3. [3]) Low CO_3. [4]) Medium CO_3 observed in "ultramafic" waters. [5]) Maximum CO_3 observed in "ultramafic" waters. [6]) Similar to mean river water according to STUMM and MORGAN (1970).

Table 5 C. Rock-fluid pairs for which dissolution processes have been calculated, based on the simple model, not considering supersaturation

	CO_3-bearing fluids			
CO_3-free fluids	Monomineralic rocks		Composite rocks	
R1/F1	R1/F2	R2/F2	R5/F2	R6/F2
R2/F1	R1/F3	R2/F3	R5/F3	R6/F3
R3/F1	R1/F4	R2/F4	R5/F4	R6/F4
R4/F1			R5/F5	R6/F5
R5/F1	R3/F2	R4/F2	R5/F6	R6/F6
R6/F1	R3/F3	R4/F3		
	R3/F4	R4/F4		

"ultramafic" waters, because those concentrations cannot increase during the dissolution calculations, unless carbonate or sulphate had been included in the reacting rocks, which was not the case. Na and K have then been adjusted to ensure electrical neutrality in the starting solution. The low diopside content in most model rocks was chosen to demonstrate that also low clinopyroxene contents can lead to a high Ca-water (see below).

2.1. Model not considering supersaturation

Although this model assumption is obviously not obeyed at surface conditions, it nevertheless shows the ideal behavior and allows a better understanding of the influence of the above mentioned control factors. Of the many runs performed (table 5c), only those for model-peridotites and model-serpentinites, dissolved by solutions of different CO_3-content, will be given here (fig. 3–5).

The peridotite dissolution path reaches, instead of overall equilibrium (with forsterite, diopside and enstatite), a "steady" state, in which the fluid solution composition stays invariant, i.e. all peridotite material that is dissolved, is directly used to form the corresponding stable assemblage at surface conditions: brucite-chrysotile (-monticellite). The calculated serpentinite dissolution path, on the other hand, reaches overall equilibrium (simultaneous precipitation of chrysotile and diopside). The calculated final pH-value is lower here (11.1–11.25) than for the peridotite dissolution (12.5).

Decreasing CO_2-contents in the initial fluid moves reaction paths to higher $a_{Mg^{2+}}/a_{H^{+2}}$-ratios and to lower a_{SiO_2}-values. As a consequence, calculated paths with CO_2-contents equal or less 10 mg/l (F1, F2, F3, table 5) did not lead to

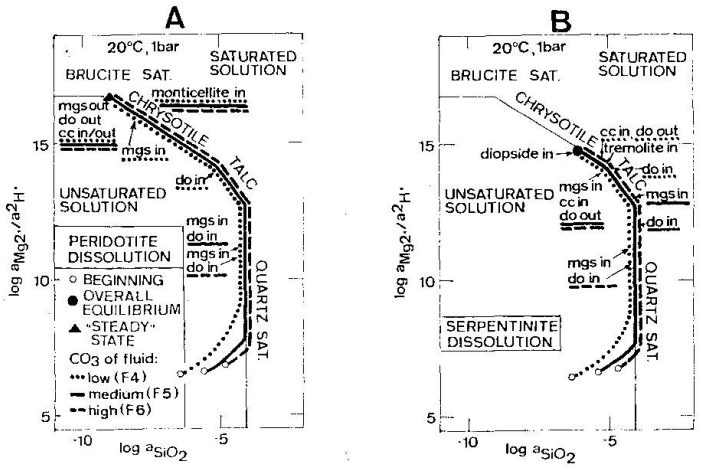

Fig. 3. Simple dissolution model, supersaturation not considered: calculated reaction paths for composite model rocks reacting with fluids of different CO_3-contents, shown on a logarithmic activity diagram (compare fig. 1). A: peridotite model rock (R5), B: serpentinite model rock (R8). The appearance of the different carbonates is marked with the following abbreviations: cc calcite, do dolomite, mgs magnesite.

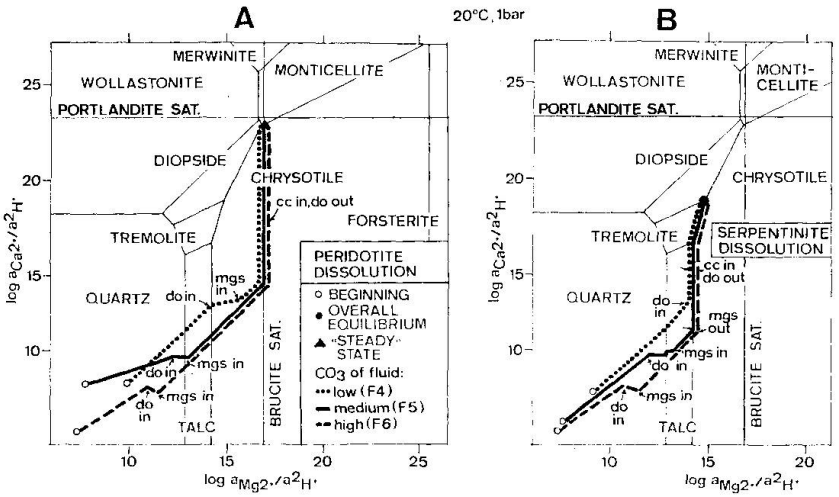

Fig. 4. Simple dissolution model, supersaturation not considered: reaction paths for composite rocks in terms of Ca and Mg of the fluid, shown on a activity diagram portraying saturation as projected planes (equilibria written with SiO_2 conserved in the solid phases). For carbonate abbreviations see fig. 3. A: peridotite model rock (R 5), B: serpentinite model rock (R 8).

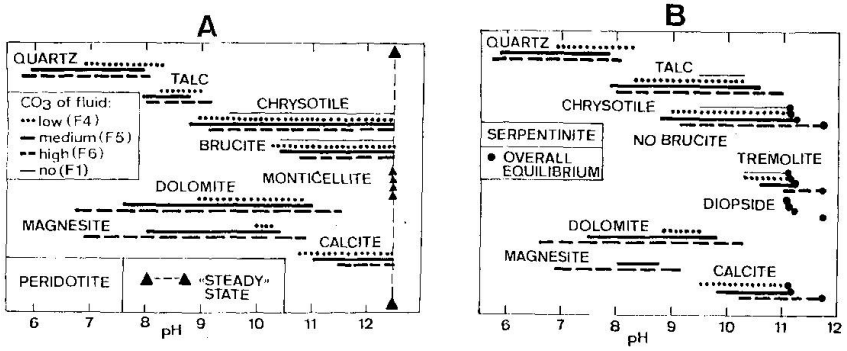

Fig. 5. Simple dissolution model, supersaturation not considered: pH at the appearance of different minerals as a function of the CO_3-content in the fluid solution. A: peridotite, B: serpentinite.

quartz nor to carbonate mineral saturation, but directly to talc- or chrysotile-saturation.

2.2. Model considering supersaturation

The saturation test of the naturally observed ultramafic fluids suggested that they are controlled by only a few mineral/fluid equilibria: silica minerals (mainly quartz), forsterite, a hypothetical serpentine phase ("chrysotile-asbestos"), carbonate minerals, except dolomite, and a Ca-silicate, possibly wollastonite. Therefore, model calculations were performed with identical rock and fluid compositions as before (table 5), but allowing the solution to get supersaturated with respect to all but the above mentioned mineral phases. This seems to correspond to the natural situation.

In addition, the effect of a non-isochemical development of the dissolution process was studied. In the former computer runs, product minerals were dis-

Table 6. Model considering supersaturation: dissolution of a peridotite model-rock by a CO_3-bearing solution (F5/R5 in table 5), assuming a non-isochemical process (see text)

Corresponding graphs: figures 6, 7 and 8.

	log ξ	pH	log f_{CO_2}	Minerals in/out	mg/l SiO_2	log a_{SiO_2}	mg/l Mg^{2+}	log $a_{Mg^{2+}}/a^2_{H^+}$	mg/l Ca^{2+}	log $a_{Ca^{2+}}/a^2_{H^+}$	mg/l CO_3^{2-}
	–	5.7	−1.05	–	0.6×10^{-5}	–	0.4	–	1.3	–	245
A	−4.10	5.88	−1.09	quartz in	4.91	−4.09	4.11	7.87	1.36	7.17	245
B	−3.07	7.98	−2.64	magnesite in	5.02	−4.09	39.93	13.00	1.99	11.46	245
C	−2.78	9.22	−4.42	calcite in	6.77	−4.09	7.85	14.78	2.62	14.10	76.88
D	−2.73	9.96	−5.59	chrys.-asbest. in	14.93	−4.09	4.43	15.95	1.39	15.27	39.03
	−2.73	9.96	−5.59	quartz out	14.93	−4.09	4.43	15.95	1.39	15.27	39.03
E	−2.43	10.88	−7.4	artinite in	0.17	−6.80	4.53	17.76	1.29	17.08	18.66
	−2.43	10.88	−7.4	magnesite out	0.17	−6.80	4.53	17.76	1.29	17.08	18.66
F	−2.39	10.96	−7.63	forsterite in	0.13	−7.02	4.10	17.90	1.59	17.35	13.75
	−2.39	10.96	−7.63	artinite out	0.13	−7.02	4.10	17.90	1.59	17.35	13.75
	−1.38	11.37	−9.63	–	0.31	−7.02	0.66	17.90	20.13	19.31	1.11
G	−0.84	11.89	−11.30	wollastonite in	1.05	−7.02	0.11	17.90	102.91	20.98	0.47
H	−0.78	11.89	−11.30	calcite out:	1.05	−7.02	0.11	17.90	102.91	20.98	0.47

"steady" state: {enstatite, diopside, water} → {chrysotile-asbestos, wollastonite}

Total mass transfer: see figure 7.

Table 7. Model considering supersaturation: dissolution of a serpentinite model rock by a CO_3-bearing fluid (F5/R5), assuming a non-isochemical process

log ξ	pH	log f_{CO_2}	Minerals in/out	mg/l SiO_2	log a_{SiO_2}	mg/l Mg^{2+}	log $a_{Mg^{2+}}/a^2_{H^+}$	mg/l Ca^{2+}	log $a_{Ca^{2+}}/a^2_{H^+}$	mg/l CO_3^{2-}
0	5.7	−1.05	–	0.6×10^{-5}	–	0.4	–	1.3	–	245.76
−4.39	5.84	−1.07	quartz in	4.91	−4.09	3.18	7.68	1.46	7.12	245.76
−3.25	7.99	−2.65	magnesite in	5.02	−4.09	39.0	13.00	3.57	11.74	245.76
−3.03	8.7	−3.67	calcite in	5.74	−4.09	14.71	14.02	5.06	13.34	123.12
−2.90	9.96	−5.59	chrysotile-asbestos in	14.97	−4.09	4.43	15.95	1.38	15.27	39.05
−2.90	9.96	−5.59	magnesite out	14.97	−4.09	4.43	15.95	1.38	15.27	39.05
−2.18	10.57	−7.55	quartz out	45.92	−4.09	0.23	15.95	6.72	17.23	3.55
−2.17	10.79	−8.39	wollastonite in	69.60	−4.11	0.09	15.97	17.25	18.07	1.4
−2.16	10.78	−8.37	quartz back in,	71.11	−4.09	0.09	15.95	17.42	18.05	1.4

calcite out: "steady" state corresponding to the univariant reaction:
{diopside, water} → {chrysotile-asbestos, wollastonite, quartz}

Total mass transfer at the end of the run (g/kg H_2O):

minerals	dissolved	precipitated
chrysotile	0.31	0.12
diopside	0.26	–
quartz	–	0.16
magnesite	–	0.28
calcite	–	0.08
wollastonite	–	0.67×10^{-3}

solved again at partial equilibrium if the saturation condition was not satisfied anymore. That way, all which had been removed from the fluid was added to it again upon dissolution. A non-isochemical process can be approximated by assuming that the fluid flows and therefore can not dissolve its own deposits anymore when saturation is lost. However, since the amounts of minerals formed and possibly dissolved later are usually quite small (table 6 and 7, fig. 7), the difference in solution composition in such "open system" runs does not change the process significantly. Usually only the amounts of product minerals that form during a certain intervall of the progress variable are slightly decreased for an "open system" run.

Of the many computer runs performed, only two examples are given here, both non-isochemical runs (peridotite- and serpentinite dissolution, table 6 and 7, fig. 6, 7 and 8). For both the final saturation state is given in appendix 4A. The first one, the model peridotite dissolution, offers a possibility how, first of all, Mg-HCO_3-waters can develop from peridotite interaction (stage A–D in table 6 and fig. 7) and secondly how Ca-OH-waters develop from Mg-HCO_3-waters (fig. 6, stage E–G in table 6): the solution follows quartz saturation up to the hypothetical chrysotile-asbestos saturation, which seems to correspond to the upper limit for water from serpentinite rocks (compare second run, table 7). Then the solution composition takes off towards forsterite saturation, continuously precipitating hypothetical chrysotile-asbestos, and becomes enriched in calcium because diopside is still dissolving (though eventually supersaturated). When forsterite saturation is reached, then only enstatite and diop-

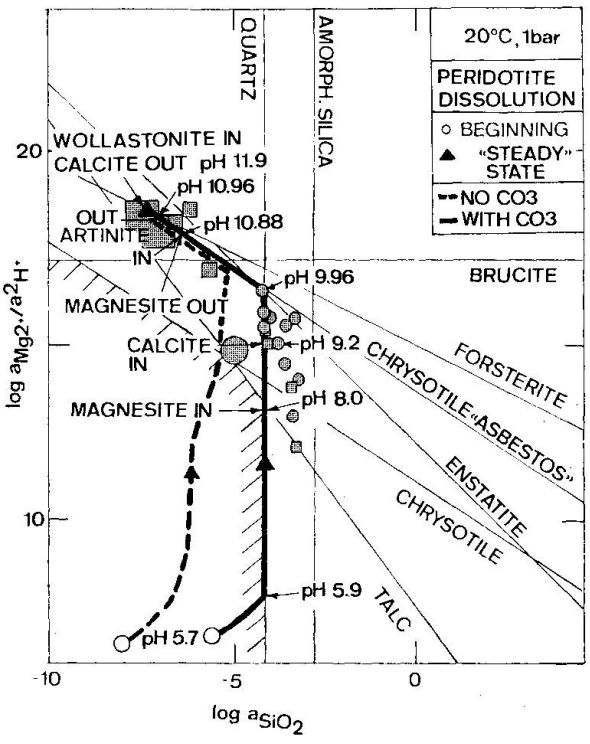

Fig. 6. Second dissolution model, supersaturation considered: calculated reaction paths for the dissolution of a peridotite model rock by a carbonate bearing fluid (245 mg/liter CO_3^{2-}, F5/R5, full line in figure) and by a carbonate-free fluid (F1/R5, dashed line in figure). Shaded symbols correspond to observed water compositions (cf. fig. 1). A non isochemical process is assumed (fluid flows, see text). Compare with table 6. Instead of using the hypothetical "chrysotile-asbestos" phase as shown on this figure, R. GARRELS suggested (pers. communication), to use NAUMOV's value for enstatite in TARDY and GARRELS (1977), which would place the enstatite saturation line below the one shown here, but would intersect the forsterite-line at the same location as "chrysotile-asbestos" does and where most Ca-OH-waters are located. It could therefore control the fluid path instead of "asbestos". However, as a consequence, also several waters from serpentinite areas would then be supersaturated with NAUMOV's enstatite, which seem to be quite unlikely.

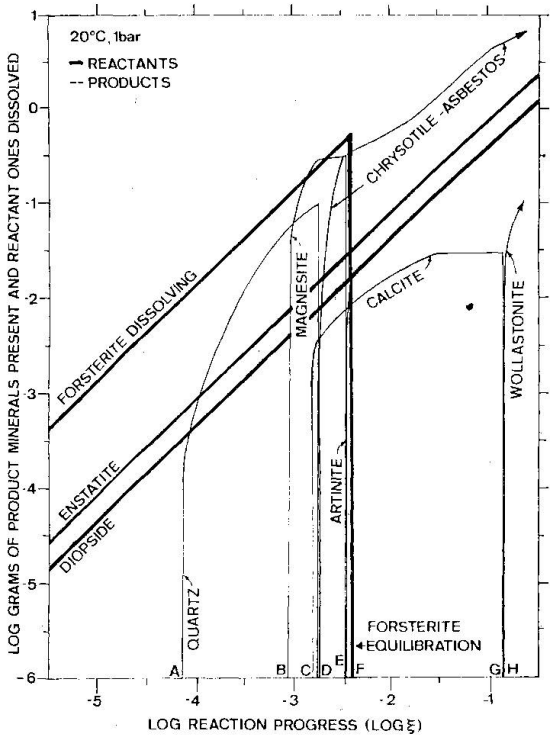

Fig. 7. Calculated mass transfer from dissolved rock to the solution and to precipitating minerals for the peridotite dissolution process of fig. 6 and table 6, shown as a function of reaction progress (ξ). Vertical lines point to very small amounts ($\lim_{M \to 0} \log M = -\infty$, M: mass).

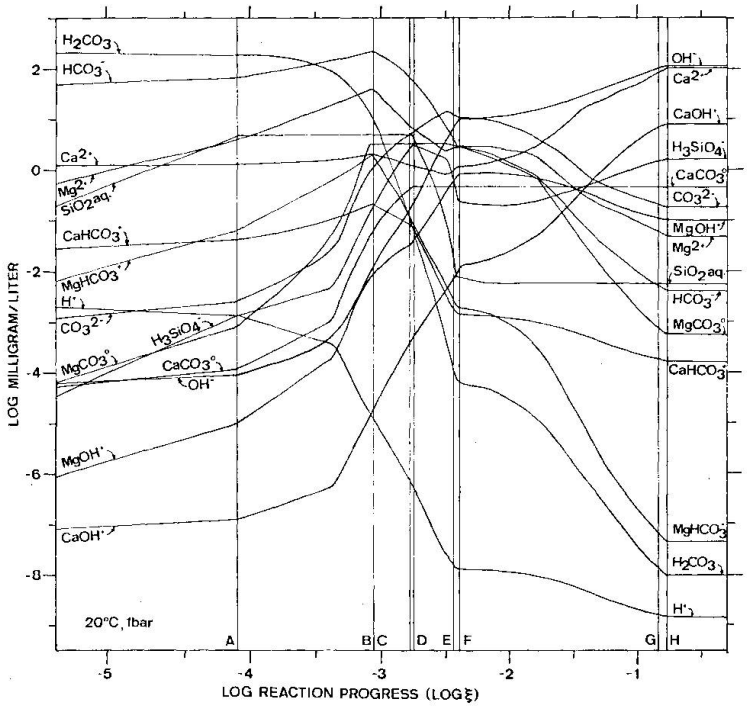

Fig. 8. Calculated concentrations of major fluid solution species during the dissolution of a model peridotite by a carbonate bearing solution (F 5 in table 5) as a function of reaction progress. Letters at the bottom refer to important events (appearance and disappearance of phases) also marked in fig. 7 and table 6.

side are dissolving, adding more silica than magnesium to the solution and driving its composition away from forsterite saturation, back towards Mg-HCO_3-compositions. As soon as saturation with forsterite is lost, but forsterite still present in the parent rock, it will again dissolve to restore equilibrium with the fluid solution. If, however, such a water moves on its way to the surface

through e.g. a serpentinite-shell, where there is no forsterite but diopside, it might easily move back on the asbestos saturation line to quartz saturation and resemble a Mg-HCO_3-type water except for carbonate.

This run also explains the absence of carbonate in the Ca-OH-waters: the carbonate could get lost through precipitation of carbonate minerals. The calculated total carbonate (as CO_3^{2-}) is close to the analytical detection limit. On the other hand, waters with Ca-OH-composition can as well form by interaction of a pure carbonate-free rain water with a peridotite rock. However, this is unlikely because in the soil layer organic CO_2 is usually added to such water before it reaches the rock. Such a carbonate-free dissolution path is nevertheless indicated in fig. 6.

The final solution of the second run, the model-serpentinite dissolution (table 7), shows strikingly similar pH, Mg-, Si- and Ca-contents and a similar degree of supersaturation as the natural water from Val Plavna, Switzerland (sample 1, table 2, serpentinite area). Different CO_3^{2-}-contents in the starting fluid and other rock compositions led, for both serpentinite and peridotite model rocks, to similar results when supersaturation was considered. It is important to note that in nature, none of the above calculated processes must go as far as shown here. If the fluid is isolated from its host rock or if one of the reactant minerals is used up or armoured, the process will obviously stop or change its path.

3. MIXING CALCULATIONS

To change a Ca-OH-water to a Mg-HCO_3-type, Ca and pH have to be lowered, CO_3, Mg and SiO_2 increased. One possible back reaction was mentioned above (addition of CO_2). However, it is difficult to model it as a whole, including all of these changes. Program SOLSAT and a few hand calculations allow to determine how much CO_2 had to be added in order to reach (1) equilibrium with the atmosphere ($pCO_2 \approx 10^{-3.5}$) and (2) saturation with calcite at pH = 9, the average value for Mg-HCO_3-waters. E.g. for sample No. 20 (Red Mountain, Blackbird Valley), a CO_2-input of about 300 mg/l and 100 mg calcite precipitation per liter was calculated. Through the strong pH-drop caused by adding CO_2, the solution even reached approximate saturation with quartz. The calculated new solution composition is as follows: pH 9.0, Ca 1.43, Mg 0.06, Na 22, K 54, Cl 26, SO_4 0.5, CO_3 370, Al 0.1, SiO_2 3.2, pCO_2 $10^{-3.55}$. The correspondance with some of the Mg-HCO_3-waters is good except for Mg and SiO_2 whose totals were not modelled and are still the same as in the original Ca-OH-water (No. 20, table 2). Sample 1, Val Plavna, seems to exhibit such mixing effects (compare footnote 2 in table 2).

4. VALIDITY OF THE DISSOLUTION MODEL

Aluminium as impurity in minerals certainly influences the real dissolution process in nature, e.g. as clay minerals and zeolithes, which could also buffer SiO_2. The effect of Fe is probably, as outlined above, limited on the redox state of the fluid. What kind of rôle silica minerals and chrysotile-asbestos really play during these processes could only be revealed through careful studies of deposits on cracks *inside* the ultramafic aquifer, which are usually not accessible.

F. Summary and conclusions

The compositions of natural fluids issuing from ultramafic rocks at surface conditions are quite different from other subsurface waters. They seem to be controlled by only a few stable and metastable fluid-mineral equilibria: CO_2-bearing waters (Mg-HCO_3-type) are determined by stable carbonate- and silica-mineral/solution equilibria but being in a disequilibrium state with hydrous Mg-silicates (supersaturated with serpentines, talc, sepiolite). CO_2-free waters (Ca-OH-type) are usually determined by metastable equilibrium with anhydrous Mg- and Ca-silicates (forsterite, enstatite, wollastonite).

The unusual high pH-values of both water types are due to the special position of these equilibria in the high pH-region. Subsurface waters from other rocks do usually not reach that high pH-values because their appropriate saturation boundaries are reached before the hydrolysis-type of dissolution process increased pH that much. pH of 12 in ultramafics can only be reached through the above mentioned metastable equilibrium state. A stable equilibrium state between fluid and ultramafic rock would correspond to pH values close to 11.

The commonest type is the Mg-HCO_3-water which can either stem from serpentinite dissolution or from mixing of a Ca-OH-water with atmospheric CO_2 at surface. Carbon dioxide-free waters from serpentinites are apparently rare and are then probably buffered by a silica-, a serpentine- and a Ca-silicate-phase (e.g. sample 1, Val Plavna). The Ca-OH-type, which is usually only found in peridotite-areas is less common, because of its highly metastable state (olivine saturation, O_2 low, CO_2-free). High Ca reflects the inability to reach equilibrium with clinopyroxene (supersaturation) and calcite (no carbonate present).

Whether or not present day serpentinization occurs at surface conditions, as BARNES and O'NEIL (1969) suggested is difficult to prove. Theoretically at least, not only Ca-OH-waters would be suitable for that, as the same authors concluded. The potential of these waters to form silica-carbonate, ophicarbonate and serpentinite rocks is probably only effective at higher than the observed temperatures. However, it can be shown with theoretical activity diagrams for the studied system (similar to fig. 1–5) for higher P- and T-conditions that the

described and modeled dissolution and equilibration processes will not change their character up to 200° C and some 100 bars. It can be expected that reaction processes will approach stable equilibrium (e.g. with brucite-serpentine or serpentine-talc, instead of metastable forsterite-enstatite) at higher metamorphic conditions, because reaction rates will be less influenced by activation energy. This effect and the increasing ion product of water (HELGESON and KIRKHAM, 1976, fig. 2) will probably lower the pH of fluids in ultramafic rocks by 3 to 5 units for such conditions.

Acknowledgement

I wish to thank V. TROMMSDORFF, who encouraged me to undertake this study. His field assistance in Val Malenco is also gratefully acknowledged. Without the computer programs and data compilations of H. C. HELGESON's group in Berkeley, this study could not have been undertaken. Critical reviews and discussions with R. GARRELS, P. PFEIFER, W. STUMM, A. B. THOMPSON, V. TROMMSDORFF and A. ZINGG contributed and clarified a lot. H. ZOBRIST in W. STUMM's water research group (EAWAG Dübendorf, Switzerland) supervised the analytical procedures and provided instruments for field measurements. I. BARNES introduced me to the Californian springs on a inspirating field trip and contributed many helpful ideas. O. HÖGL, Berne, drew my attention to the Val Plavna spring. J. P. FANZUN, Tarasp, assisted during sampling there. This work was supported by the Schweizerische Nationalfonds (grant No. 2.616-0.76). The Zentenarfonds of ETH-Zürich provided funds to publish this manuscript. Their support is gratefully acknowledged.

References

BARNES, I. and F. E. CLARKE (1969): Chemical properties of ground water and their corrosion and encrustation effects on wells. U.S. Geol. Surv. Prof. Pap. 498-D, 58 p.

BARNES, I. and J. R. O'NEIL (1969): The relationships between fluids in some fresh alpine-type ultramafics and possible modern serpentinization, Western United States. Geol. Soc. Am. Bull. 80, 1947–1969.

— (1971): Calcium-magnesium carbonate solid solutions from Holocene conglomerate cements and travertines in the Coast Range of California. Geochim. Cosmochim. Acta 35, 699–718.

BARNES, I. et al. (1972): Metamorphic assemblages and the direction of flow of metamorphic fluids in four instances of serpentinization. Contr. Min. Petrol. 35, 263–276.

— (1973): Silica-carbonate alteration of serpentine: Wall rock alteration in mercury deposits of the Californian Coast ranges. Econ. Geol. 68, 388–390.

BODENLOS, A. J. (1950): Geology of the Red Mountain magnesite district, Santa Clara and Stanislaus counties, California. Calif. Jour. Mines and Geol. 46, 223–278.

BUCHER, K. und H. R. PFEIFER (1973): Über Metamorphose und Deformation der östlichen Malenco-Ultramafitite und deren Rahmengesteine. Schweiz. mineral. petrogr. Mitt. 53, 231–242.

BUTLER, J. N. (1964): Ionic equilibrium. Addison Wesley, Reading, Mass., 547 p.

CADISCH, J., A. EUGSTER und E. WENK (1968): Erläuterungen zum Blatt 44, Scuol/Schuls-Tarasp, Geol. Atlas Schweiz 1 : 25000, Schweiz. Geol. Komm.

DE QUERVAIN, F. (1976): Dolomit, Aragonit und Magnesit im Serpentin von Tarasp. Schweiz. Strahler, 89–95.

Droubi, A., C. Cheverry, B. Fritz et Y. Tardy (1976): Géochimie des eaux et des sels dans les sols des polders du lac Tchad: Applications d'un modèle thermodynamique de simulation de l'évaporisation. Chem. Geol. 17, 165–177.

Droubi, A., B. Fritz et Y. Tardy (1976): Equilibres entre minéraux et solutions. Programmes de calcul appliqués à la prédiction de la salure des sols et des doses optimales d'irrigation. Cah. ORSTROM, Sér. Pédol 14, 13–38.

Eugster, H. P. (1977): Compositions and thermodynamics of metamorphic solutions. 183–202, in D. G. Fraser (ed.), Thermodynamics in geology. Reidel, Dordrecht, Holland, 410 p.

Fehlmann, H. (1919): Der schweizerische Bergbau während des Weltkrieges. Kümmerly & Frey, Bern, p. 284–287.

Folk, R. L. and E. F. McBridge (1976): Possible pedogenic origin of Ligurian ophicalcite: A mesozoic calichified serpentinite. Geology 4, 327–332.

Fritz, B. (1975): Etude thermodynamique et simulation des réactions entre minéraux et solutions. Application à la géochimie des altérations et des eaux continentales. Thèse Univ. Strasbourg, 152 p.

Garrels, R. M. and F. T. Mackenzie (1971): Evolution of sedimentary rocks. W. Norton Co., New York, 397 p.

Gramaccioli, C. M. (1962): I minerali valtellinesi nella raccolta di Pietro Sigismund. Milano, 179 p.

Greenwood, H. J. (1967): Mineral equilibria in the system MgO-SiO_2-H_2O-CO_2, p. 542–567 in: P. H. Abelson (ed.): Researches in geochemistry: vol. 2. John Wiley and Sons, New York, 663 p.

Harnik, A. B. und G. Harnik (1976): Tobermorit, eine Modellsubstanz für synthetische Kalziumsilikathydrate. Schweiz. mineral. petrogr. Mitt. 56, 145–160.

Helgeson, H. C. (1967): Solution chemistry and metamorphism, 362–404, in: P. H. Abelson, ed., Advances in geochemistry, vol. 2, John Wiley, New York, 663 p.

— (1968): Evaluation of irreversible reactions in geochemical processes involving minerals and aqueous solutions. I. Thermodynamic relations. Geochim. Cosmochim. Acta 32, 853–877.

— (1969): Thermodynamics of hydrothermal systems at elevated temperatures and pressures. Am. J. Sc. 267, 729–804.

— (1970): A chemical and thermodynamic model of ore deposition in hydrothermal systems. Min. Soc. Amer. Spec. Pap. 3, 155–186.

— (1971): Kinetics of mass transfer among silicates and aqueous solutions. Geochim. Cosmochim. Acta 35, 421–469.

— (1974): Chemical interaction of feldspars and aqueous solutions, p. 184–217 in: The feldspars, proc. NATO adv. Study Inst., Manchester 1972, editors: W. S. Mackenzie, J. Zussmann. Manchester Univ. Press.

Helgeson, H. C., T. H. Brown, A. Nigrini and T. A. Jones (1970): Calculation of mass transfer in geochemical processes involving aqueous solutions. Geochim. Cosmochim. Acta 34, 569–592.

Helgeson, H. C., T. A. Jones, T. Mundt, T. H. Brown, A. Nigrini, R. H. Leeper and D. H. Kirkham (1971, ms.): PATH1 and databank PATDAT, program No. 1000, comp. library H. C. Helgeson, U. C. Berkeley, USA.

Helgeson, H. C. and D. H. Kirkham (1974a): Theoretical prediction of the thermodynamic behavior of aqueous electrolytes at high pressures and temperatures: I. Summary of the thermodynamic electrostatic properties of the solute. Am. J. Sci. 274, 1089–1198.

— (1974b): Theoretical prediction of the thermodynamic behavior of aqueous electrolytes

at high pressures and temperatures: II. Debye-Hückel parameters for activity coefficients and relative partial molal properties. Am. J. Sci. 274, 1199–1261.

— (1976): Theoretical prediction of the thermodynamic behavior of aqueous electrolytes at high pressures and temperatures: III. Equation of state for aqueous species at infinite dilution. Am. J. Sci. 276, 97–240.

Helgeson, H. C., J. Delany and W. Nesbitt (1978): Summary and critique of thermodynamic properties of rock-forming minerals. Am. J. Sci. (in press).

Hemley, J. J., J. W. Montoya, C. L. Christ and P. B. Hostetler (1977): Mineral equilibria in the MgO-SiO_2-H_2O system: I. Talc-chrysotile-forsterite-brucite stability relations. Am. J. Sci. 277, 322–351.

Hemley, J. J., J. W. Montoya, D. R. Shaw and R. W. Luce (1977): Mineral equilibria in the MgO-SiO_2-H_2O-system: II. Talc-antigorite-forsterite-anthophyllite-enstatite stability relations and some geological implications in the system. Am. J. Sci. 277, 353–383.

Holloway, J. R. (1977): Fugacity and activity of molecular species in supercritical fluids. 161–181 in D. G. Fraser (ed.), Thermodynamics in geology. Reidel, Dordrecht, Holland, 410 p.

Johannes, W. (1969): An experimental investigation of the system MgO-SiO_2-H_2O-CO_2. Am. J. Sci. 267, 1083–1104.

— (1975): Zur Synthese und thermischen Stabilität von Antigorit. Fortschr. Mineral. 53, 36.

Kharaka, Y. K. and I. Barnes (1973): SOLMNEQ: Solution-mineral equilibrium computations. U.S. Geol. Survey Computer Cont., NTIS report PB-215 899.

Kirkham, D. H., J. V. Walther and J. Delany (1975, ms.): SUPCRT, a Fortran IV-computer program to compute the thermodynamic properties of minerals, gases and aqueous species and/or equilibrium constants etc. at elevated pressures and temperatures. Program No. 7402, Computer library H. C. Helgeson, U. C. Berkeley.

Leeper, R. H. (1969, ms.): SOLSAT, a Fortran IV-program to compute the distribution of species in aqueous solutions and to define the extent to which the solution is saturated or supersaturated with minerals. Program No. 0711, program library H. C. Helgeson, U. C. Berkeley.

Moody, J. (1976): Serpentinization, a review. Lithos 9, 125–238.

Nesbitt, H. W. (1974, ms.): The study of some mineral-aqueous solution interactions. Ph. D. Thesis, John Hopkins Univ. Baltimore, 180 p.

Plummer, N. L., B. F. Jones and A. H. Truesdell (1976): WATEQF, a Fortran IV-version of WATEQ, a computer program for calculating chemical equilibrium of natural water. U.S. Geol. Surv. Water-Resources investigat. 76-13.

Poty, B., H. D. Holland and M. Borcsik (1972): Solution-mineral equilibria in the system MgO-SiO_2-H_2O-$MgCl_2$ at 500° C and 1 kbar. Geochim. Cosmochim. Acta 36, 1101–1113.

Roedder, E. (1965): Liquid CO_2-inclusions in olivine bearing nodules and phenocrysts from basalts. Am. Mineral 50, 1956–1982.

— (1972): Composition of fluid inclusions. U.S. Geol. Surv. Prof. Pap. 440-JJ: Data of Geochemistry, 6th edition. 164 p.

Schweizerisches Lebensmittelbuch (1972): Chapter 27, Trinkwasser.

Stumm, W. and J. Morgan (1970): Aquatic chemistry. Wiley Interscience, New York, 583 p.

Tarnuzzer, Ch. und U. Grubenmann (1909): Beiträge zur Geologie des Unterengadins. Beitr. Geol. Karte Schweiz, Lf. 23, 245–248.

Tardy, Y. and R. M. Garrels (1977): Prediction of Gibbs energies of formation of compounds from the elements. II. Monovalent and divalent metal silicates. Geochim. Cosmochim. Acta 41, 87–92.

TAYLOR, H. F. W. (1968): The calcium silicate hydrates. Symp. Chem. Cem. Tokyo, sess. 2-1, 1–26.

TROMMSDORFF, V. and B. EVANS (1977): Antigorite-ophicarbonates: Phase relations in a portion of the system CaO-MgO-SiO_2-H_2O-CO_2. Contr. Mineral. Petrol. 60, 39–56.

TRUESDELL, A. H. and B. F. JONES (1974): WATEQ, a computer program for calculating chemical equilibria of natural waters. J. Res. U.S. Geol. Surv. 2, n. 2, 233–248.

WALTHER, J. V. and H. C. HELGESON (1977): Calculation of the thermodynamic properties of aqueous silica and the solubility of quartz and its polymorphs at high pressures and temperatures. Am. J. Sci. (in press).

WALTERS, L. J. and T. J. WOLERY (1975): A monotone sequence algorithm and Fortran IV-program for calculation of equilibrium distributions of chemical species. Comp. Geosci. 1.

Appendix 1

Basic assumptions and equations used for the interpretation of natural water analyses (species distribution model of program SOLSAT)

A. Biogenic influences are neglected.

B. The aqueous fluid is a dilute electrolyte solution consisting of the slightly polarized solvent H_2O and as aqueous species free ions, electrically charged or neutral complexes and molecules. NaCl is the main (supporting) electrolyte (HELGESON, 1969).

C. The species distribution (speciation) is only determined by predominantly homogeneous equilibria among the chosen species (see appendix 2) and is calculated by simultaneous solution of mass action equations for the chosen fluid equilibria, the electroneutrality equation and total mass equations (mass balances) for each of the involved elements:

$$\sum_i \nu_i A_i = 0, \tag{1}$$

which is the conservation law for a chemical reaction process, where A_i: mass or chemical potential (only at equilibrium), ν_i: reaction coefficient, $\nu = -|\nu|$ for reactants, $\nu = |\nu|$ for products.

$$\Delta G_r^\circ(P,T) = -RT\ln K(P,T) \tag{2}$$

corresponds to the free energy change of reaction, where R: gas constant, T: absolute temperature, P: pressure, K: equilibrium constant. Calculation of P,T-dependance of ΔG_r and K based on data given in HELGESON (1969).

$$K = \prod_i (\gamma_i m_i)^{\nu_i} = \prod_i (a_i)_{eq}^{\nu_i} \tag{3}$$

expresses the mass action law, where K: equilibrium constant, i: index of aqueous species, m_i: molality (mole/kg H_2O), γ_i: individual ion activity coefficient, a_i: activity.

Standard states used: For H_2O: a = 1 if pure, at any P and T. For CO_2, O_2, H_2, etc.: ideal gas at P = 1 bar and T of interest, i.e. a = f/1, therefore $a_{gas} = f_{gas}$ (f: fugacity). For aqueous species: hypothetical one molal solution at any P and T, i.e. $\gamma_i \to 1$ if $m_i \to 0$.

$$\sum_i m_i z_i = 0 \tag{4}$$

is the electroneutrality equation where z_i is the electrical charge.

$$m_{tot,j} = \sum_i \lambda_i m_i \tag{5}$$

is the total mass equation for each element, where j: index of elements, λ_i: number of the j-th element in the i-th species.

Calculation of γ_i (Debye-Hückel theory):

For ions:

$$\log \gamma_i(P,T) = -\frac{A(P,T) z_i^2 \bar{I}^{1/2}}{1 + \mathring{a}_i B(P,T) \bar{I}^{1/2}} + b(P,T)\bar{I}, \tag{6a}$$

$$A(P,T) = \frac{1.825 \times 10^6 \rho_{H_2O}(P,T)}{[\epsilon_{H_2O}(P,T)T]^{3/2}}, \tag{6b}$$

$$B(P,T) = \frac{50.292 \times 10^8 [\rho_{H_2O}(P,T)]^{1/2}}{[\epsilon_{H_2O}(P,T)T]^{1/2}}, \tag{6c}$$

where ϵ_{H_2O}, ρ_{H_2O}: dielectric constant and density of H_2O respectively, after HELGESON and KIRKHAM (1974b), $\mathring{a}_i$: hydrated ion size (distance of closest approach) of which the data is taken from BUTLER (1964, p. 434), b(P,T): deviation function, assumed to be independant of species other than NaCl, i.e. taken for pure NaCl-solutions (HELGESON, 1969), $\bar{I}$: true (nonstoichiometric) ionic strength which is calculated by:

$$\bar{I} = 1/2 \sum_i m_i z_i^2. \tag{6d}$$

For neutral species (HELGESON, 1969):

$$\gamma_i = \gamma_{CO_2}(m_{NaCl}, P, T). \tag{7}$$

Exception: $\gamma_{SiO_2 aq.} = 1$.

Redox equilibria: calculated from SO_4^{2-} and HS^- determinations with the following reaction relation:

$$O_2(g) + 0.5\,HS^- = 0.5\,H^+ + 0.5\,SO_4^{2-} \tag{8}$$

and for Me^{3+}/Me^{2+} pairs (e.g. Fe^{3+}/Fe^{2+}) reactions of the type

$$Me^{3+} + 0.125\,HS^- + 0.5\,H_2O = 1\,Me^{2+} + 0.125\,SO_4^{2-} + 1.125\,H^+ \tag{9}$$

are used.

Activity of H_2O:

$$a_{H_2O} = 1 \text{ for dilute solutions } (m_{NaCl,tot} < 0.25). \tag{10}$$

For more concentrated solutions:

$$\ln a_{H_2O} = \frac{2 m_{NaCl,tot} \Phi_{NaCl}(P,T)}{55.5}, \tag{11}$$

where $\Phi_{NaCl}(P,T)$: molal osmotic coefficient of NaCl, interpolated for actual $m_{NaCl,tot}$ from table 2 in HELGESON (1969).

D. Relationship between fluid solution and rock:

$$Q = IAP = \prod_i a_i^{\nu_i}: \text{ which is the ion activity product.} \tag{12}$$

It is assumed that equilibrium between minerals and the fluid solution is reached through hydrolysis reactions of the type given in appendix 3.

$$\text{Saturation with respect to minerals: } Q(P,T) = K(P,T), \tag{13a}$$

$$\text{supersaturation: } Q > K, \tag{13b}$$

$$\text{undersaturation: } Q < K. \tag{13c}$$

Measurement of the saturation state is done with:

$$\Delta(\Delta G_r) = RT(\ln Q - \ln K), \tag{14}$$

where $\Delta(\Delta G_r) = 0$: saturation,

$\Delta(\Delta G_r) > 0$: supersaturation,

$\Delta(\Delta G_r) < 0$: undersaturation.

Solid solution in minerals (binary with the two endmember indices h and l, cf. HELGESON et al., 1970):

$$a_j = \frac{\prod_s a_s^{\nu_{s,j}}}{K_j} = \frac{Q_j}{K_j}, \text{ where } j = h \text{ or } l \tag{15}$$

and a: activity, ν: reaction coefficient, K: equilibrium constant, Q: ion activity product.

Activity can be expressed as:

$$a_j = \lambda_j X_j, \quad j = h \text{ or } l, \tag{16}$$

where X: mole fraction, λ: rational activity coefficient. In addition holds:

$$X_h + X_l = 1. \tag{17}$$

For *regular* solid solutions:

$$\ln\lambda_h = -\frac{1}{RT}\left(\frac{W_h'' X_l^2}{2} + \frac{W_h''' X_l^3}{3}\right), \tag{18a}$$

$$\ln\lambda_l = -\frac{1}{RT}\left(\frac{W_h'' X_h^2}{2} + \frac{W_h''' X_h^3}{3}\right). \tag{18b}$$

From (16) and (18) follows:

$$a_h = X_h \exp\left[-\frac{1}{RT}\left(\frac{W_h''(1-X_h)^2}{2} - \frac{W_h'''(1-X_h)^3}{3}\right)\right]. \tag{19}$$

For a solid solution phase which can be described with a regular solution model (18), first of all a hypothetical a_h is calculated from (15) and then used in (19) to calculate X_h. X_l follows from (17), which allows then to calculate λ_l with (18b) and then a_l with the help of (16). a_l is then used to calculate

$$Q_l = a_l^{-1} \prod_s a_s^{\nu_{s,j}}, \tag{20}$$

which can then be checked with K_l for saturation [cf. (13), (14)].

For *ideal* solid solutions:

$$W''_h = W'''_h = 0 \quad \text{and therefore}$$
$$\lambda_h = \lambda_l = 1 \quad \text{and therefore}$$
$$a_h = X_h \quad \text{and} \quad a_l = X_l. \tag{21}$$

Hypothetical $a_h = X_h$ are calculated from

$$X_h = \frac{Q_h/Q_l}{K_h/K_l + Q_h/Q_l}, \tag{22}$$

which can be derived from a_h/a_l with (15) and the condition that $a_h + a_l = 1$.

E. Program set up: As in most of these programs, the distribution calculation in SOLSAT is based on an iteration of the ionic strength calculation, which starts with $\gamma = 1$ and ionic strength $I = 0$ and hence activities equal to total molalities. In an inner loop the non-linear equation system is solved with successive substitution into the different mass action- and other equations. After each cycle, the total mass equations (6) for carbonate and sulfur are checked, and if the calculated values are close enough to the analyzed ones, a new ionic strength (10) and subsequent γ's (7) are calculated and the appropriate new activities are then used to recalculate the species distribution. The calculation stops if two successive ionic strength calculations do only differ by a small choosable amount. If, after this speciation calculation, the electrical neutrality (5) does not hold anymore, it is adjusted by adding or subtracting Cl^- to the solution.

Appendix 2

Equilibria considered among aqueous and gaseous species in the fluid phase

A. The data for the dissociational equilibria for the following aqueous species were taken from HELGESON (1969, table 4 and 5):

H_2O, KSO_4^-, $NaCl^\circ$, $CaCO_3^\circ$, $CaSO_4^\circ$, $MgSO_4^\circ$, $MnSO_4^\circ$, HSO_4^-, HS^-, H_2S°, HCO_3^-, $H_2CO_3^*$, HCl°, $Mg(OH)^+$, $Al(OH)^{2+}$, $Al(OH)_4^-$, $Fe(OH)^+$, $FeCl^{2+}$, $FeCl_2^+$, $FeCl_3$, $FeCl_4^-$. * apparent $H_2CO_3 = CO_2\,aq. + H_2CO_3^\circ$

B. The data for the following species were taken from HELGESON et al. (1971):

$NaCO_3^-$, $NaSO_4^-$, $CaHCO_3^+$, $MgCO_3^\circ$, $Ca(OH)^+$, $Fe(OH)^{2+}$

C. The following equilibria were calculated with program SUPCRT (KIRKHAM et al, 1975, see also appendix 3):

$SiO_2\,aq. + 2H_2O = H_3SiO_4^- + H^+$: $\log K\,(25^\circ C, 1\,bar) = -9.65$

$S_2(g) + 2H_2O = 1.5HS^- + 0.5SO_4^{2-} + 2.5H^+$: $\log K\,(25^\circ C, 1\,bar) = 7.15$

$O_2(g) + 0.5HS^- = 0.5H^+ + 0.5SO_4^{2-}$: $\log K\,(25^\circ C, 1\,bar) = 66.28$

Appendix 3

Reaction equations used for saturation check and log K-values at 25° C for comparison

Log K values without footnotes (and their PT-variation) are calculated with program SUPCRT (KIRKHAM et al., 1975) based on data from HELGESON and KIRKHAM (1974a, 1976), WALTHER and HELGESON (1977), HELGESON, DELANY and NESBITT (1978) and HOLLOWAY (1977)

		log K 25°, 1 bar
Fe-Al-free minerals		
Akermanite:	$Ca_2MgSi_2O_7 + 6H^+ = 2Ca^{2+} + Mg^{2+} + SiO_2aq. + 3H_2O$	45.4
Amorphous silica:	$SiO_2 = SiO_2aq.$	−2.71
Anhydrite:	$CaSO_4 = Ca^{2+} + SO_4^{2-}$	−4.15
Antigorite:	$Mg_{2.82}Si_2O_5(OH)_{3.65} + 5.65H^+ = 2.82Mg^{2+} + 2SiO_2aq. + 4.65H_2O$	29.32[1])
Mg-Anthophyllite:	$Mg_7Si_8O_{22}(OH)_2 + 14H^+ = 7Mg^{2+} + 8SiO_2aq. + 8H_2O$	67.79
Aragonite:	$CaCO_3 = Ca^{2+} + CO_3^{2-}$	−8.36
Artinite:	$Mg_2(OH)_2CO_3 \cdot 3H_2O + 2H^+ = 2Mg^{2+} + CO_3^{2-} + 5H_2O$	9.59
Brucite:	$Mg(OH)_2 + 2H^+ = Mg^{2+} + 2H_2O$	16.44
Chalcedony:	$SiO_2 = SiO_2aq.$	−3.73
Calcite:	$CaCO_3 = Ca^{2+} + CO_3^{2-}$	−8.36
Chrysotile:	$Mg_3Si_2O_5(OH)_4 + 6H^+ = 3Mg^{2+} + 2SiO_2aq. + 5H_2O$	31.55/38.88[7])
Dolomite:	$CaMg(CO_3)_2 = Ca^{2+} + Mg^{2+} + 2CO_3^{2-}$	−18.06
Diopside:	$CaMgSi_2O_6 + 4H^+ = Ca^{2+} + Mg^{2+} + 2SiO_2aq. + 2H_2O$	21.08
Enstatite:	$MgSiO_3 + 2H^+ = Mg^{2+} + SiO_2aq. + H_2O$	11.47
Epsomite:	$MgSO_4 \cdot 7H_2O = Mg^{2+} + SO_4^{2-} + 7H_2O$	−2.14[2])
Forsterite:	$Mg_2SiO_4 + 4H^+ = 2Mg^{2+} + SiO_2aq. + 2H_2O$	28.15
Gypsum:	$CaSO_4 \cdot 2H_2O = Ca^{2+} + SO_4^{2-} + 2H_2O$	−4.85
Huntite:	$Mg_3Ca(CO_3)_4 = Ca^{2+} + 3Mg^{2+} + 4CO_3^{2-}$	−30.52
Hexahedrite:	$MgSO_4 \cdot 6H_2O = Mg^{2+} + SO_4^{2-} + 6H_2O$	−1.69[2])
Hydromagnesite:	$Mg_4(CO_3)_4(OH)_2 \cdot 4H_2O + 2H^+ = 5Mg^{2+} + 4CO_3^{2-} + 6H_2O$	−9.82
Kenyaite:	$NaSi_{11}O_{20.5}(OH)_4 \cdot 3H_2O + H^+ = Na^+ + 11SiO_2aq. + 5.5H_2O$	−25.0[3])
Magadiite:	$NaSi_7O_{13}(OH)_3 \cdot 3H_2O + H^+ = Na^+ + 7SiO_2aq. + 5H_2O$	−14.3
Magnesite:	$MgCO_3 = Mg^{2+} + CO_3^{2-}$	−7.91
Merwinite:	$Ca_3Mg(SiO_4)_2 + 8H^+ = 3Ca^{2+} + Mg^{2+} + 2SiO_2aq. + 4H_2O$	68.57
Monticellite:	$CaMgSiO_4 + 4H^+ = Ca^{2+} + Mg^{2+} + SiO_2aq. + 2H_2O$	29.86
Nesquehonite:	$MgCO_3 \cdot 3H_2O = Mg^{2+} + CO_3^{2-} + 3H_2O$	4.99
Periclase:	$MgO + 2H^+ = Mg^{2+} + H_2O$	21.48
Portlandite:	$Ca(OH)_2 + 2H^+ = Ca^{2+} + 2H_2O$	22.6[4])
Quartz (α):	$SiO_2 = SiO_2aq.$	−4.0[8])
Rhodochrosite:	$MnCO_3 = Mn^{2+} + CO_3^{2-}$	−10.54
Sepiolite:	$Mg_4Si_6O_{15} \cdot 7H_2O + 8H^+ = 4Mg^{2+} + 6SiO_2aq. + 11H_2O$	31.0
Talc:	$Mg_3Si_4O_{10}(OH)_2 + 6H^+ = 3Mg^{2+} + 4SiO_2aq. + 4H_2O$	21.56
Tremolite:	$Ca_2Mg_5Si_8O_{22}(OH)_2 + 14H^+ = 2Ca^{2+} + 5Mg^{2+} + 8SiO_2aq. + 8H_2O$	61.88
Wollastonite:	$CaSiO_3 + 2H^+ = Ca^{2+} + SiO_2aq. + H_2O$	13.73
Al-bearing minerals		
Analcime:	$NaAlSi_2O_6 \cdot H_2O + 4H^+ = Na^+ + Al^{3+} + 2SiO_2aq. + 3H_2O$	9.41
Boehmite:	$AlO(OH) + 3H^+ = Al^{3+} + 2H_2O$	8.78
Clinochlore (7 Å):	$Mg_5AlAlSi_3O_{10}(OH)_8 + 16H^+ = 5Mg^{2+} + 2Al^{3+} + 3SiO_2aq. + 12H_2O$	70.81
Clinochlore (14 Å):	$Mg_5AlAlSi_3O_{10}(OH)_8 + 16H^+ = 5Mg^{2+} + 2Al^{3+} + 3SiO_2aq. + 12H_2O$	67.15
Clinozoisite:	$Ca_2Al_3Si_3O_{12}(OH) + 13H^+ = 2Ca^{2+} + 3Al^{3+} + 3SiO_2aq. + 7H_2O$	40.55
Diaspore:	$AlO(OH) + 3H^+ = Al^{3+} + 3H_2O$	7.93

		log K 25°, 1 bar
Gibbsite:	$Al(OH)_3 + 3H^+ = Al^{3+} + 3H_2O$	7.25
Grossular:	$Ca_3Al_2Si_3O_{12} + 12H^+ = 3Ca^{2+} + 2Al^{3+} + 3SiO_2aq. + 6H_2O$	51.86
Illite:	$K_{0.6}Mg_{0.25}Al_{2.3}Si_{3.5}O_{10}(OH)_2 + 8H^+ = 2.3Al^{3+} + 0.6K^+ + 3.5SiO_2aq. + 5H_2O$	10.34[4]
Kaolinite:	$Al_2Si_2O_5(OH)_4 + 6H^+ = 2Al^{3+} + 2SiO_2aq. + 5H_2O$	6.30
Laumontite:	$CaAl_2Si_4O_{12} \cdot 4H_2O + 8H^+ = Ca^{2+} + 2Al^{3+} + 4SiO_2aq. + 8H_2O$	14.42
Ca-Montmorillonite:	$Ca_{0.167}Al_{2.33}Si_{3.67}O_{10}(OH)_2 + 7.33H^+ = 0.167Ca^{2+} + 2.33Al^{3+} + 3.67SiO_2aq. + 4.67H_2O$	6.2[4]
K-Montmorillonite:	$K_{0.33}Al_{2.33}Si_{3.67}O_{10}(OH)_2 + 7.33H^+ = 0.33K^+ + 2.33Al^{3+} + 3.67SiO_2aq. + 4.67H_2O$	6.11[4]
Mg-Montmorillonite:	$Mg_{0.167}Al_{2.33}Si_{3.67}O_{10}(OH)_2 + 7.33H^+ = 0.167Mg^{2+} + 2.33Al^{3+} + 3.67SiO_2aq. + 4.67H_2O$	6.10[4]
Na-Montmorillonite:	$Na_{0.33}Al_{2.33}Si_{3.67}O_{10}(OH)_2 + 7.33H^+ = 0.33Na^+ + 2.33Al^{3+} + 3.67SiO_2aq. + 4.67H_2O$	6.35[4]
Phlogopite:	$KMg_3AlSi_3O_{10}(OH)_2 + 10H^+ = K^+ + 3Mg^{2+} + Al^{3+} + 3SiO_2aq. + 6H_2O$	40.46
Prehnite:	$Ca_2AlAlSi_3O_{10}(OH)_2 + 10H^+ = 2Ca^{2+} + 2Al^{3+} + 3SiO_2aq. + 6H_2O$	34.73
Wairakite:	$CaAl_2Si_2O_{12} \cdot 2H_2O + 8H^+ = Ca^{2+} + 2Al^{3+} + 4SiO_2aq. + 6H_2O$	17.8
Zoisite:	$Ca_2Al_3Si_3O_{12}(OH) + 13H^+ = 2Ca^{2+} + 3Al^{3+} + 3SiO_2aq. + 7H_2O$	40.59
Fe-bearing minerals		
Ferroactinolite:	$Ca_2Fe_5Si_8O_{22}(OH)_2 + 14H^+ = 2Ca^{2+} + 5Fe^{2+} + 8SiO_2aq. + 8H_2O$	36.32
Andradite:	$Ca_3Fe_2Si_3O_{12} + 12H^+ = 3Ca^{2+} + 2Fe^{2+} + 3SiO_2aq. + 6H_2O$	24.98
Fayalite:	$Fe_2SiO_4 + 4H^+ = 2Fe^{2+} + SiO_2aq. + H_2O$	15.31
$Fe(OH)_2$ amorphous:	$Fe(OH)_2 = Fe^{2+} + 2OH^-$	−15.09[2]
$Fe(OH)_3$ amorphous:	$Fe(OH)_3 = Fe^{3+} + 3OH^-$	−4.98[5]
Ferrosilite:	$FeSiO_3 + 2H^+ = Fe^{2+} + SiO_2aq. + H_2O$	5.85
Goethite:	$FeO(OH) + H_2O = Fe^{3+} + 3OH^-$	−41.2[5]
Greenalite:	$Fe_3Si_2O_5(OH)_4 + 6H^+ = 3Fe^{2+} + 2SiO_2aq. + 5H_2O$	17.54[6]
Hematite:	$Fe_2O_3 + 6H^+ = 2Fe^{3+} + 3H_2O$	−4.05
Hedenbergite:	$CaFe(SiO_3)_2 + 4H^+ = Ca^{2+} + Fe^{2+} + 2SiO_2aq. + 2H_2O$	15.56
Magnetite:	$Fe_3O_4 + 8H^+ = Fe^{2+} + 2Fe^{3+} + 4H_2O$	3.83
Minnesotaite:	$Fe_3Si_4O_{10}(OH)_2 + 6H^+ = 3Fe^{2+} + 4SiO_2aq. + 4H_2O$	7.24[6]
Pyrite:	$FeS_2 + H_2O = Fe^{2+} + 0.25SO_4^{2-} + 1.75HS^- + 0.25H^+$	−26.88
Siderite:	$FeCO_3 = Fe^{2+} + CO_3^{2-}$	−12.73

[1]) Retrieved from JOHANNES (1975) with data of HELGESON, DELANY and NESBITT and the condition that antigorite is stable with respect to talc and chrysotile only above 200° C at one bar. [2]) FRITZ (1975). [3]) DROUBI et al. (1976). [4]) HELGESON (1969). [5]) TRUESDELL and JONES (1974). [6]) Provisional, HELGESON, personal communication 1976. [7]) Hypothetical chrysotile-asbestos. [8]) WALTHER and HELGESON (1977).

Appendix 4A

Saturation state of known waters issuing from ultramafic rocks with respect to Mg-Ca-minerals, expressed as $\Delta(\Delta G)$, in kcal, from equilibrium value
(cf. appendix 1, part D)

Numbers on top correspond to spring localities in table 1, except 24 and 25, which correspond to the final computed fluid solutions for peridotite and serpentinite dissolution by an originally carbonate-bearing fluid (see text). + : supersaturation; − : undersaturation.

	1	2	3	4	5	6	7	8	9	10	11	12
Antigorite	+ 7.65	+ 5.83	+ 4.61	+ 3.40	− 1.97	+10.23	+ 7.08	+ 2.13	− 1.89	+ 2.90	+ 4.57	+ 2.84
Brucite	− 1.66	− 2.38	− 2.92	− 3.31	− 4.55	− 1.37	− 2.39	− 4.44	− 5.71	− 3.82	− 3.08	− 3.92
Halite	− 9.08	− 8.58	−12.56	−10.75	−12.19	−11.36	−10.74	−11.92	−12.77	−11.85	−11.62	−11.96
Sylvite	− 9.89	− 9.33	−12.03	+ 1.05	−11.83	−12.34	−11.05	−11.43	−12.71	−11.84	−11.84	−12.40
Calcite	−	+ 1.71	+ 1.08	+ 1.19	+ 1.40	+ 1.51	+ 1.32	+ 0.16	− 1.35	− 0.20	− 0.02	+ 0.62
Magnesite	−	− 1.28	+ 1.63	+ 4.48	+ 1.60	+ 3.02	+ 2.40	+ 0.43	− 0.69	− 0.02	+ 1.13	+ 1.06
Dolomite	−	+ 2.66	+ 4.95	− 5.40	+ 5.24	+ 6.81	+ 5.96	+ 2.82	+ 0.19	+ 2.00	+ 3.34	+ 3.90
Hydromagnesite	−	−14.50	− 3.25	− 4.73	− 4.92	+ 3.39	+ 0.12	− 9.80	−15.56	−11.01	− 5.65	− 7.01
Anhydrite	− 3.24	− 5.50	− 4.95	− 3.59	− 5.57	− 5.85	− 5.13	− 5.97	− 5.35	− 5.41	− 5.63	− 5.54
Gypsum	− 2.12	− 4.38	− 3.81	+ 0.22	− 4.41	− 4.89	− 4.05	− 4.90	− 4.28	− 4.43	− 4.55	− 4.58
Quartz	0.007	+ 0.11	+ 0.27	+ 3.23	− 0.69	+ 0.84	+ 0.74	+ 1.15	+ 0.95	+ 0.67	+ 0.45	+ 0.75
Sepiolite	+ 8.41	+ 6.19	+ 5.10	+ 3.76	− 7.11	−14.24	+ 0.79	+ 4.08	− 2.27	+ 3.63	+ 5.32	+ 3.48
Chrysotile, normal	+ 8.30	+ 6.35	+ 5.04	− 6.24	− 1.81	+10.90	− 7.59	+ 2.28	− 1.96	+ 3.16	+ 4.96	+ 3.07
Chrysotile-asbestos	− 1.70	− 3.63	− 4.96	+ 6.80	−11.81	+ 0.9	− 2.41	− 7.72	−11.96	− 6.84	− 5.03	− 6.93
Talc	+10.93	+ 9.20	+ 8.18	− 3.07	− 0.62	+15.30	+11.73	+ 7.24	+ 2.58	+ 7.15	+ 8.52	+ 7.27
Artinite	−	− 4.74	− 2.74	− 4.92	− 3.79	+ 0.20	− 1.19	− 5.20	− 7.60	− 5.04	− 3.14	− 4.31
Tremolite	+23.60	+16.99	+ 7.25	− 1.91	−11.34	+21.46	+13.93	+ 4.52	− 6.85	+ 5.14	+ 6.69	+ 4.88
Enstatite	− 0.45	− 1.06	− 1.47	− 2.19	− 4.11	+ 0.79	− 0.40	− 2.04	− 3.52	− 1.91	− 1.38	− 1.85
Diopside	+ 5.09	+ 2.65	− 1.71	− 5.93	− 6.60	+ 1.83	− 0.14	− 2.60	− 5.96	− 2.25	− 2.16	− 2.44
Wollastonite	− 0.11	− 1.95	− 5.89	− 5.71	− 8.16	− 4.59	− 5.38	− 6.21	− 8.08	− 5.98	− 6.43	− 6.22
Forsterite	− 2.55	− 3.88	− 4.87	+ 2.21	− 9.18	− 0.90	− 3.20	− 6.88	− 9.64	− 6.13	− 4.86	− 6.09
Huntite	−	− 4.55	+ 3.57	− 1.63	+ 3.77	+ 8.28	+ 6.14	− 0.93	− 5.80	− 2.66	+ 0.98	+ 1.44
Amorphous silica	− 1.82	− 1.71	− 1.58	+ 0.83	− 2.57	− 0.91	− 1.06	− 0.65	− 0.56	− 1.13	− 1.35	− 1.01
Aragonite	−	+ 1.49	+ 0.87	−10.34	− 1.19	+ 1.34	+ 1.10	− 0.06	− 1.57	− 0.04	− 0.24	+ 0.39
Periclase	− 8.65	− 9.37	− 9.95	− 0.15	−11.62	− 8.25	− 9.35	−11.39	−12.67	−10.78	−10.03	−10.79
Chalcedony	− 0.36	− 0.25	− 0.01	− 1.36	− 1.06	+ 0.47	− 0.37	+ 0.78	+ 0.57	+ 0.30	+ 0.08	+ 0.38
Mg-Anthophyllite	+ 8.65	+ 4.48	+ 1.79	−31.04	−17.56	+18.00	+ 9.62	− 1.40	−12.00	− 0.97	+ 2.52	− 0.60
Merwinite	−11.66	−17.99	−30.59	− 8.97	−38.13	−25.45	−28.87	−33.81	−40.49	−32.04	−32.40	−32.80
Monticellite	− 1.47	− 4.03	− 8.55	−17.45	−12.49	− 5.54	− 7.43	−10.30	−13.45	− 9.46	− 9.16	− 9.72
Akermanite	− 4.12	− 8.50	−16.99	−22.10	−23.22	−12.60	−15.33	−19.03	−24.04	−17.96	−18.10	−18.41
Nesquehonite	−	−32.38	−21.38	− 7.02	−22.94	−21.43	−21.00	−24.00	−25.56	−25.18	−23.11	−24.0
Hexahedrite	− 9.41	−10.44	− 6.19	− 6.46	− 6.38	− 6.90	− 6.18	− 7.83	− 6.82	− 7.36	− 6.61	− 7.60
Epsomite	− 8.82	− 9.86	− 5.62	− 6.46	− 5.81	− 6.29	− 5.59	− 7.23	− 6.23	− 6.77	− 6.01	− 6.98
Kenyaite	−18.34	−16.63	−20.58	−32.05	−20.21	− 9.40	−12.11	− 9.04	−12.57	−14.36	−16.15	− 5.06
Magadiite	−10.05	− 8.77	−12.95	−20.17	−12.38	− 5.54	− 7.14	− 5.71	− 8.41	− 9.10	−10.02	− 4.87
Rhodochrosite	−	−	− 0.1	+ 1.02	−	−	−	−	−	−	−	−
Portlandite	− 6.80	− 8.75	−12.80	−14.04	−12.78	−12.16	−14.08	−14.08	−15.74	−13.37	−13.60	−13.70

	13	14	15	16	17	18	19	20	21	22	23	24	25
Antigorite	+ 5.59	− 1.00	+ 5.95	+ 8.40	+ 8.77	+ 9.39	−11.98	− 8.45	+12.69	+ 6.65	+ 9.46	+11.41	+ 8.77
Brucite	− 2.30	− 5.57	− 2.27	+ 1.43	+ 1.88	+ 0.51	+ 1.71	+ 0.72	+ 1.60	− 3.07	− 2.64	− 1.12	+ 1.50
Halite	−12.60	−12.59	−12.03	−10.83	−10.03	−10.09	− 9.53	− 9.49	− 3.18	− 3.98	− 3.69	− 9.03	− 9.07
Sylvite	−13.54	−12.79	−12.94	−11.68	−11.40	−10.89	−10.75	− 8.12	− 4.32	− 5.11	− 5.02	− 8.96	− 9.0
Calcite	+ 0.28	− 0.32	+ 0.56	–	–	–	–	–	+ 0.25	+ 0.99	+ 0.63	0	0
Magnesite	+ 1.27	+ 0.006	+ 1.92	–	–	–	–	–	− 0.68	− 1.12	− 0.87	− 3.72	− 5.05
Dolomite	+ 3.76	+ 1.91	+ 4.71	–	–	–	–	–	+ 1.81	+ 2.107	+ 1.99	− 1.49	− 1.41
Hydromagnesite	− 4.58	−12.64	− 1.82	–	–	–	–	–	− 8.09	−14.53	−13.09	−23.22	−25.92
Anhydrite	− 7.85	− 6.81	− 5.61	− 6.14	–	–	− 5.33	− 5.85	− 7.35	− 6.94	− 7.56	− 4.52	− 3.74
Gypsum	+ 6.89	− 5.73	− 4.59	− 5.12	–	–	− 4.25	− 4.73	− 6.24	− 5.82	− 6.44	− 3.50	− 2.73
Quartz	− 0.16	+ 1.19	− 0.009	− 4.00	− 4.49	− 2.24	− 2.62	− 2.98	− 2.10	+ 1.48	+ 2.27	0	− 3.93
Sepiolite	+ 4.50	− 0.25	+ 5.65	− 3.52	− 4.61	+ 3.2	+ 6.00	+ 0.01	+ 8.82	+11.61	+18.09	+10.35	− 2.76
Chrysotile, normal	− 6.10	− 1.05	+ 6.47	+ 9.58	+ 9.97	+10.36	+13.16	− 9.47	+13.87	+ 7.01	+ 9.89	+ 9.97	+ 9.97
Chrysotile-asbestos	− 3.90	−11.05	− 3.52	− 0.42	− 0.02	+ 0.34	+ 3.17	− 0.53	+ 3.88	− 2.98	− 0.10	0	0
Talc	+ 8.49	+ 3.97	+ 9.14	+ 4.25	+ 3.68	+ 8.56	−10.565	+ 6.12	+12.29	+12.59	+17.05	+12.65	+ 4.79
Artinite	− 2.48	− 6.76	− 1.68	–	–	–	–	–	− 0.15	− 5.27	− 4.58	− 6.17	− 4.87
Tremolite	+ 7.84	− 3.25	+ 8.40	+12.53	−12.41	−21.30	−25.32	+17.65	−23.00	+21.32	+29.43	+26.74	+16.28
Enstatite	− 1.14	− 3.14	− 0.99	− 1.29	− 1.32	− 0.42	+ 0.33	− 1.05	+ 0.71	− 0.38	+ 0.84	+ 0.17	− 1.14
Diopside	− 1.57	− 4.86	− 1.62	+ 2.89	+ 3.11	+ 5.12	+ 6.13	+ 4.52	+ 4.11	+ 3.12	+ 4.94	+ 5.80	+ 4.50
Wollastonite	− 6.06	− 7.36	− 6.26	− 1.45	− 1.20	− 0.09	+ 0.16	− 0.08	− 2.25	− 2.15	− 1.55	0	0
Forsterite	− 3.77	− 9.11	− 3.63	− 0.23	+ 0.19	− 0.24	+ 1.63	− 0.77	+ 1.87	− 3.90	+11.76	− 1.32	0
Huntite	+ 1.71	− 2.69	+ 3.94	–	–	–	–	–	− 4.18	− 4.77	− 4.37	−13.53	−17.53
Amorphous silica	− 1.92	− 0.61	− 1.79	− 5.78	− 6.26	− 4.00	− 4.42	− 4.81	− 3.93	− 0.35	+ 0.44	− 1.87	− 5.70
Aragonite	+ 0.05	− 0.54	+ 0.34	–	–	–	–	–	+ 0.03	+ 0.78	+ 0.41	− 0.21	− 0.22
Periclase	− 9.18	−12.52	− 9.19	− 5.49	− 5.04	− 6.37	− 5.25	− 6.27	− 5.39	−10.06	− 9.63	− 8.04	− 5.41
Chalcedony	− 0.53	+ 0.82	− 0.38	− 4.37	− 4.86	− 2.62	− 2.99	− 3.35	− 2.47	+ 1.11	+ 1.90	− 0.36	− 4.30
Mg-Anthophyllite	+ 3.45	− 9.06	+ 4.68	− 1.40	− 2.09	+ 6.40	+11.40	+ 1.42	+14.62	+10.56	+19.92	+12.86	− 0.25
Merwinite	−29.78	−38.44	−30.56	− 8.46	− 6.76	− 6.97	− 4.79	− 6.19	−12.70	−20.66	−19.21	−10.69	− 4.09
Monticellite	− 7.94	−12.59	− 8.15	+ 0.36	+ 1.06	+ 0.84	+ 2.21	+ 0.95	− 0.35	− 4.92	− 3.88	− 0.75	+ 1.89
Akermanite	−16.46	−22.47	−16.90	− 3.59	− 2.63	− 1.72	− 0.15	−16.64	− 5.13	− 9.60	− 7.96	− 3.25	− 0.60
Nesquehonite	−24.50	−24.27	−22.53	–	–	–	–	–	−31.33	−34.54	−33.94	−36.01	−38.10
Hexahedrite	− 9.37	− 8.61	− 6.58	−12.21	–	–	−11.18	−12.67	−10.23	−11.00	−11.00	−10.57	−11.10
Epsomite	− 8.76	− 8.01	− 5.97	−11.60	–	–	−10.59	−12.08	− 9.65	−10.42	−10.42	− 9.97	−10.50
Kenyaite	−20.83	− 9.45	−19.69	−59.50	−63.94	−39.23	−44.67	−49.81	−36.69	+ 0.79	+ 9.83	−15.66	−57.49
Magadiite	−12.95	− 6.26	−12.08	−35.91	−38.42	−23.00	−26.24	−29.56	−19.97	+ 3.19	+ 9.06	− 8.12	−34.19
Rhodochrosite	+ 0.39	− 1.36	+ 0.25	–	–	–	–	–	–	–	–	–	–
Portlandite	−12.62	−15.27	−12.98	− 4.18	− 3.44	− 4.56	− 3.94	− 3.78	− 6.83	−10.31	−10.50	− 6.75	− 2.80

Appendix 4B

Saturation state of some "ultramafic" waters with respect to some Al-bearing phases

Mineral	Sample number 16	18	19	20
Laumontite	−12.19	− 3.94	− 5.70	− 7.84
Gibbsite	− 0.55	+ 0.21	− 0.13	− 0.90
Analcime	−11.13	− 6.77	− 7.44	− 9.20
Kaolinite	− 8.90	− 3.81	− 5.36	− 7.77
Na-Montmorillonite	−17.99	− 9.55	−11.93	−15.26
Muscovite	−11.90	− 4.08	− 6.42	− 7.53
Illite	−14.34	− 6.39	− 8.52	−10.51
Zoisite	− 2.43	+ 4.51	+ 3.27	− 0.006
Prehnite	− 3.70	+ 2.41	+ 1.63	− 0.82
Phlogopite	+ 6.61	+10.11	+12.12	+ 9.59
K-Montmorillonite	−18.31	− 9.85	−12.39	−14.86
Ca-Montmorillonite	−17.12	− 8.76	−11.23	−14.48
Mg-Montmorillonite	−17.49	− 9.19	−11.60	−15.05
Wairakite	−16.91	− 8.55	−10.51	−13.54
Clinozoisite	− 2.37	+ 4.57	+ 3.33	+ 0.06
Diaspore	− 1.52	− 0.72	− 1.14	− 1.95
Boehmite	− 2.69	− 1.87	− 2.33	− 3.15
7Å-Clinochlore	+12.79	+15.14	+19.01	+11.31
14Å-Clinochlore	+17.77	+20.15	+23.97	+16.24
Grossular	− 0.32	+ 5.40	+ 5.26	+ 2.94

Appendix 4C

Saturation state of some "ultramafic" waters with respect to Fe-bearing phases

Mineral	Sample number 12	15	22	23
Goethite	+ 0.71	+ 2.27	+ 2.44	+ 2.86
$Fe(OH)_2$ am.	− 5.06	− 3.52	− 0.41	+ 0.18
$Fe(OH)_3$ am.	− 4.87	− 2.90	− 1.98	− 1.55
Pyrite	−25.25	−24.39	+14.86	+16.81
Magnetite	+10.94	+15.63	+18.98	+20.41
Hematite	+ 9.13	+12.24	+12.41	+13.26
Siderite	+ 1.69	+ 2.51	+ 3.51	+ 3.91
Ferroactinolite	+ 9.97	+13.42	+46.62	+55.50
Fayalite	− 0.48	+ 1.95	+ 9.80	+11.76
Minnesotaite	+ 8.98	+10.76	+26.38	+31.30
Andradite	+ 7.05	+10.10	+22.69	+25.36
Hedenbergite	− 0.87	− 0.06	+ 8.73	+10.71
Greenalite	+ 4.38	+ 7.68	+20.38	+23.72
Ferrosilite	− 0.13	+ 0.71	+ 5.38	+ 6.75

Appendix 4D

Saturation state with respect to some hypothetical solid solution minerals compared with pure end members

Data used: An ideal model was assumed for forsterite-fayalite, tremolite-ferroactinolite, talc-minnesotaite and chrysotile-greenalite. A regular model was used for calcite-dolomite. For the latter the following rather hypothetical "solvus" data was used for 25° C, 1 bar: $X_{dol} = 0.02$–0.99 with the following Margules parameters (cf. appendix 1, part D):

$$W''_h = -12{,}708,\ W''_h = -7{,}990.$$

Sample number	Solid solution series (ss), $\Delta(\Delta G)$ in kcal				
	forst.-fay.	*trem.-ferroact.*	*talc-minnes.*	*chrys.-green.*	*calc.-dolom.*
	$X_{fay.}$	$X_{ferroact.}$	$X_{minnes.}$	$X_{green.}$	$X_{dolom.}$
	$\Delta(\Delta G)_{ss}$	$\Delta(\Delta G)_{ss}$	$\Delta(\Delta G)_{ss}$	$\Delta(\Delta G)_{ss}$	$\Delta(\Delta G)_{ss}$
	$\Delta(\Delta G)_{fay.}$	$\Delta(\Delta G)_{ferroact.}$	$\Delta(\Delta G)_{minnes.}$	$\Delta(\Delta G)_{green.}$	$\Delta(\Delta G)_{dolom.}$
12	0.99992	0.9998	0.94	0.89	1.0
	− 0.48	+ 9.97	+ 8.98	+ 4.38	+1.95
	− 0.48	+ 9.97	+ 8.95	+ 4.31	+1.95
15	1.0	1.0	0.94	0.89	1.0
	+ 1.95	+13.42	+10.80	+ 7.75	+2.35
	+ 1.95	+13.42	+10.76	+ 7.68	+2.35
22	1.0	–	1.0	1.0	1.0
	+ 9.80		+26.38	+20.38	+1.05
	+ 9.80		+26.38	+20.38	+1.05
23	1.0	–	1.0	1.0	1.0
	+11.76		+31.3	+27.72	+1.0
	+11.76		+31.3	+23.72	+1.0

Sample 2–11, 13, 14, 21: The only solid solutions which could form are carbonates (because there is no Fe in the fluid). A check resulted in supersaturation with pure dolomite-end member for all samples except for No. 2, which showed supersaturation with practically pure calcite. Appropriate $\Delta(\Delta G)$-values can be found in appendix 4A.

Appendix 5

Basic assumptions of program PATH

A. The program essentially simulates what hypothetically happens if a certain rock type (to be specified at the outset) is titrated, i.e. added in small amounts, into a fluid solution of a certain initial composition which is also specified at the outset.

B. It simulates this – as a whole, irreversible (initial rock is out of equilibrium with the initial fluid solution) – process with small steps which hold the solution in internal homogeneous equilibrium and as soon as saturation with one or more minerals is achieved or lost, the program is set up to precipitate or dissolve these minerals at *partial* or *local equilibrium*.

C. The calculation is carried out with a similar type of equation system for mass, electrical charge and mass action laws as in program SOLSAT, but written in terms of differentials like $dm_i/d\xi$, $dx_\phi/d\xi$ (where m_i: molality, x_ϕ: grams of a mineral relative to 1000 g H_2O, ξ: progress or reaction variable, see short summary in HELGESON, 1971, p. 460). The progress variable, which is proportional to the amount of original reactant rock already dissolved, is increased in steps and after each a redistribution of aqueous species and a saturation check are made, as in program SOLSAT.

D. The calculated mass transfer from rock to fluid solution and from there to newly formed minerals is always relative to 1000 g of water.

E. The solution is assumed to be homogeneous, i.e. no compositional gradients nor an explicit transport equation for diffusion, bulk transport or both have been considered. The rate limiting step (with respect to ξ) is the irreversible dissolution process, i.e. it is implicitly assumed, that equilibrium in the solution and between the solution and minerals precipitating therefrom is reached at least as quickly as the dissolution process evolves (HELGESON et al., 1970).

Manuscript received October 28, 1977.